REPORT DOCUMENTATION PAGE

Form Approved
OMB No. 0704-0188

1. AGENCY USE ONLY *(Leave blank)*	2. REPORT DATE	3. REPORT TYPE AND DATES COVERED
	14 Jan 99	Final Technical Report 01 Oct 96 to 30 Sep 98

4. TITLE AND SUBTITLE
75 Micron YAG-Alumina Eutectic Fiber

5. FUNDING NUMBERS
F49620-96-C-0047
3005/SS

6. AUTHOR(S)
Joseph M. Collins

7. PERFORMING ORGANIZATION NAME(S) AND ADDRESS(ES)
Saphikon, Inc.
33 Powers Street
Milford, NH 03055

8. PERFORMING ORGANIZATION REPORT NUMBER

9. SPONSORING/MONITORING AGENCY NAME(S) AND ADDRESS(ES)
AFOSR/NA
801 N. Randolph Street, Rm 732
Arlington, VA 22203-1977

10. SPONSORING/MONITORING AGENCY REPORT NUMBER
F49620-96-C-0047

11. SUPPLEMENTARY NOTES

12a. DISTRIBUTION AVAILABILITY STATEMENT
Approve for public releaes; distribution unlimited.

12b. DISTRIBUTION CODE

13. ABSTRACT *(Maximum 200 words)*

Crystal growth experiments were conducted to test the application of the Edge-defined Film- fed Growth (EFG*) technique to the growth of 75 mm single crystal yttrium aluminum garnet - alumina eutectic fibers (YAE) as well as off-eutectic and additive-modified eutectic fibers. The additive modifiers were selected to weaken the interface between the YAG and alumina phases and toughen the material. In combination with the off eutectic composition, it was hoped that an in-situ composite would be formed. It was determined that PrAlO4 was the best modifier, of those examined, in regards to crack deflection at the alumina-YAG interface. The CeAl12O19 modified YAE also showed some crack deflection though not as much as the PrAlO4 system. It was also determined that the alumina rich side of the pseudo-binary eutectic produced superior tensile strengths over the YAG rich side but the YAG rich side may produce better creep properties.

14. SUBJECT TERMS	15. NUMBER OF PAGES
	88
	16. PRICE CODE

17. SECURITY CLASSIFICATION OF REPORT	18. SECURITY CLASSIFICATION OF THIS PAGE	19. SECURITY CLASSIFICATION OF ABSTRACT	20. LIMITATION OF ABSTRACT
UNCLASSIFIED	UNCLASSIFIED	UNCLASSIFIED	UL

14 JAN 1999

75 Micron YAG-Alumina Eutectic Fiber

AFOSR

CONTRACT F49620-96-C-0047

Ref Saphikon PO # 5

ATTN: AFOSR/NA Dr. Alexander Pechenik

Directorate of Aerospace and Materials Science

Final Report

Submitted by:

Joseph M. Collins
Saphikon, Inc.
33 Powers Street
Milford, NH 03055

I. PROGRAM OBJECTIVE

Advanced engines inevitably require high operating temperatures to satisfy efficiency and performance goals in an increasingly competitive economic environment. This means that combustor and exhaust system components can operate at temperatures >2400 °F (1316 °C) and become limited by critical material properties such as creep, thermal fatigue, oxidation and thermal shock resistance. Thermo-oxidative stability, material cost and component manufactured cost are equally important. The application of ceramic matrix composites (CMC's) to these applications is considered essential for achieving the property and performance goals stated above.

Refractory ceramic materials which are capable of operation at the very high temperatures of interest, >1370°C (>2500°F), generally fall into one of two categories: materials which are inherently stable to oxidation (i.e. oxides), or oxidizable materials which form protective oxide films of silica. Recent theoretical[1] and experimental[1,2] work has shown that composites based on oxidizable phases within dense oxide matrices demonstrate poor oxidation resistance. The above references clearly indicate that any reinforcement for an oxide matrix must itself be inherently stable against oxidation. The only materials which meet this criterion are oxides and noble metals; however, noble metals are impractical due to their poor high temperature mechanical properties and their very high densities. **This leaves only the oxides as reinforcement candidates for oxide matrix composites.**

Presently, several types of continuous oxide fibers are commercially available. Unfortunately, the majority of these fibers are produced either from organometallic precursors (sol-gel) or by the extrusion and sintering of fine powders. The resultant fibers are typically contain thermally unstable amorphous or metastable phases. These microstructures make the fibers highly susceptible to strength degradation via crystallization or grain growth. All polycrystalline fibers show strength degradation above 800°C, and little or no strength above 1200 °C. Only oxide single crystal fibers and aligned eutectic fibers maintain a significant portion of their strength at 1370 °C and above. The relatively good high temperature strength of these melt derived fibers is a direct result of their stable structure, which eliminates the degradation mechanism mentioned above.

Even though the Saphikon EFG single crystal alumina fiber is stable at elevated temperatures, other properties make it less desirable as a fiber reinforcement. These are primarily the rapid strength loss at moderate temperatures (~400°C)[3] and the very directional nature of the creep properties of sapphire.[4] These limitations have led to the investigation of alternate fiber compositions which have the desirable qualities of sapphire but improve on its deficiencies. Foremost among these alternatives is the EFG 75μm YAG-Alumina Eutectic fiber (YAE). This composition has been shown to be very stable at elevated temperatures and mechanical testing of 150 mm YAE fibers yielded elevated temperature (1094°C (2000°F)) strengths which were ~33% stronger than sapphire fibers.[5] Furthermore the creep properties of this fiber were comparable to sapphire[5] and should show little variation with crystal orientation due to the very high creep resistance of the yttrium aluminum garnet (YAG) phase.

BACKGROUND

The YAE fibers are grown using the Edge-defined Film-fed Growth (EFG™) process. The EFG™ setup is comprised of a refractory metal crucible for containing the high purity feedstock material, with a capillary/die arrangement configured within the crucible. Induction heating is used to melt the feedstock, which rises in the capillary to the die tip, as shown in Figure 1. The outside shape of the die tip defines the shape of the crystal. For fiber growth, the die shape is circular, with a single drilled capillary in the center of the circle. Rectangular, square, and complex cross sectional shapes can also be grown with the EFG process.

A crystallographically oriented seed fiber is guided into contact with the tip. Once the tip of the seed is melted by contact with the die tip, the seed is pulled upward at a controlled rate. The crystal can then be grown continuously, with the solidifying region at the die tip being continuously replenished via capillary flow from the crucible. The entire hot zone can be enclosed in an argon atmosphere. A continuous belt puller and spooler arrangement is used to allow for the growth of fibers hundreds of meters long.

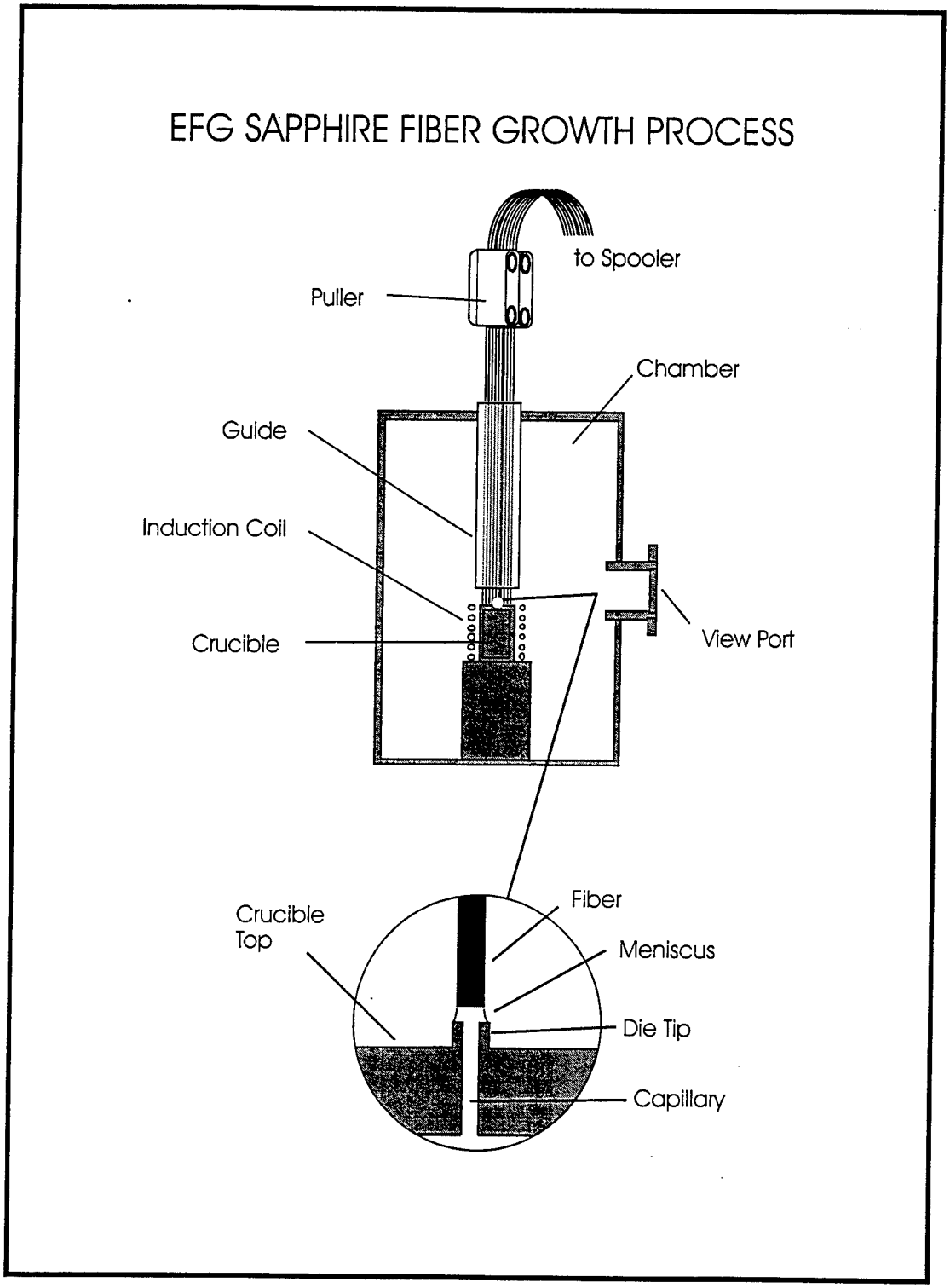

Figure 1. Schematic illustration of EFG fiber growth process.

3. PHASE II EXPERIMENTAL RESULTS

Fiber Studies:

Growth

A total of 45 EFG growth runs were made for this program, as described in Table I. Initial growth runs were made to provide fiber samples for the various evaluations. These runs consisted of YAEII001-YAEII007. The quality of these runs was generally good and room temperature tensile strengths were in the range of 1.7-2.1 GPa (250-300 Ksi). Samples of fiber were produced and distributed to the groups involved in this program for a variety of studies. These investigations will be reported individually but include, mechanical testing, long term thermo-mechanical stability and microscopy of both solidified melts and directionally solidified YAE ribbons and rods with modifiers.

The balance of the growth runs, YAEII008-YAEII045, were undertaken to extend the fiber growth process and improve the quality. The primary variables used to modify the fiber characteristics were the growth rate and fiber composition. It was difficult to grow the YAE fibers at rates > 1"/min (0.42 mm/sec) with repeatability and in fact 0.6"/min (0.25 mm/sec) was the most stable upper growth rate attainable for multi-fiber growth.

The reasons for this were threefold. The rate and temperature fluctuations which were acceptable in the 150μm fiber became more pronounced as the fiber diameter was reduced from 150μm to 75μm. It is most likely that this is due to the reduced size of the fiber and not to any changes in the growth equipment. It is possible that equipment modifications would help to mitigate these issues and some success was had when using a modified growth machine.

The second limitation was the thermal gradient across the die array. This gradient has always been present but is more detrimental to the 75μm fiber. This size appears to be more sensitive to these fluctuations than the larger diameter YAE fiber. Attempts were made to reduce this gradient but with little success. This is most likely due in part to the use of RF heating which applies the heat to the outside of the crucible and produces hot regions at the ends of the die array and cold regions in the middle of the die array.

Finally, a third limitation was the effect of melt level. As the melt level in the crucible decreased through the length of the run, the thermal gradient across the die array was increased. The result was reduce the total fiber lengths and overall run lengths. Recent results in other products have shown that there are methods such as continuous feeding which can control this effect, but the can cause other problems such as thermal perturbations need to be resolved. The continuous feed approach might be used to reduce the thermal effect of melt level but a radical new design would be needed to isolate the entering feed melt from the hot zone and specifically the die array to minimize thermal fluctuations caused by the melting of the feed material. It was not possible to do this in the limited time span of this program.

The inability to increase the growth rate limited the ability to reduce the eutectic microstructure scale. The most likely reason the growth rate could not be increased above 1"/min (0.42 mm) was most likely due to the increased instability in the growth front at the increased growth rate. This was exacerbated by the previously mentioned issues in growth.

It was expected that the increasing the growth rate would produce enhanced tensile strengths due to the finer microstructure which would be produced. The scale of the microstructure has been shown in numerous studies to be inversely related to the growth rate. It is also well documented that the scale of the microstructure has a significant influence on the fiber strength with finer microstructures having higher average tensile strengths. The inability to reduce the fiber scale limited our ability to significantly change the tensile strength using the growth rate.

Mechanical Property Data:

In general the YAE fiber had very good mechanical properties with the best values from fiber B of run YAEII026. The average tensile strength was 2.6 GPa (383 Ksi) with a standard deviation of 0.84 GPa (122 Ksi). This fiber had a very high average strength but it also had a very large standard deviation and in fact four samples failed before being tested. This could be due to the fragility of the fiber or due to handling issues.

The second best tensile strength was for run YAEII025, which had an average tensile strength of 2.6 GPa (379 Ksi) with a standard deviation of 0.45 GPa (65 Ksi). This run had a tensile strength which was almost as high as YAEII026B but had a much lower standard deviation at half the value of the YAEII 026B fiber. Due to the short length of these fibers, elevated temperature tensile test were not done. These two runs showed that high values of tensile strength may be achieved with the YAE fiber and that it can be achieved more than once.

Structure Modification Studies:

Preliminary Modifier Investigation

A total of 12 different modifiers were added to the base YAE melt to determine their stability in the YAE melt and the resultant phases which formed when the melt was solidified. The intent of this effort was to weaken the interface between the YAG and alumina phases enough to allow crack deflection and toughening. Modifiers were chosen which formed structures which have weak planes similar to those found in graphite but which are oxides. If the desired phase formed and aligned at the boundary between the YAG and alumina phases, the resulting structure had the potential to be very tough and behave like an *in-situ* composite.

Table XVIII lists the materials used to modify the YAE. A total of 5 grams of modifier were added to ~25 grams of base YAE charge. The charge was heated to ~1950°C and held for 30 minutes and then rapidly cooled to solidification by shutting of the power supply. The various compositions were first analyzed by X-ray diffraction to determine the major phases present. The modifiers which produced detectable amounts of YAP were not considered further. The only exception to this was the $SrAl_{12}O_{19}$ modifier which did not have enough alumina added in proportion to the SrO addition. The result was that alumina from the YAG phase was consumed to produce the $SrAl_{12}O_{19}$ phase and resulted in residual YAP in addition to the YAG phase.. This melt was redone with correct amounts of alumina. The second iteration of the $SrAl_{12}O_{19}$ modified YAE melt produced only the YAG, $SrAl_{12}O_{19}$, and alumina phases. It was decided to investigate this system further based on these results.

Of the other systems studied, the following were no longer considered: $LaTaO_4$, $YTaO_4$, $YNbO_4$ and $LaAlO_4$. This was due to the formation of the undesirable YAP phase. Two modifiers produced detectable levels of the desired modifier phase, these were: $SrAl_{12}O_{19}$ and $CaWO_4$. The $CaWO_4$ melt study was conducted in a sealed crucible to prevent the volatilization of the WO_3 constituent which is known to have a high vapor pressure. It was not considered feasible to directionally solidify the YAE with the $CaWO_4$ modifier while preventing the evaporation of the WO_3 constituent and this composition was not considered further.

The remaining modifiers, $NdAlO_4$, $PrAlO_4$, $CaAl_{12}O_{19}$, $CeAl_{12}O_{19}$, $LaNbO_4$, and Al_2TiO_5, were studied with SEM and TEM microscopes at Northwestern University to determine whether the desired modifier phase was present and if it produced the crack deflection at the phase boundaries which might produce significant toughening. The samples were indented to produce cracks and these were inspected. Based on this work the $PrAlO_4$ and $CeAl_{12}O_{19}$ phases were chosen for more study due to the presence of crack deflection at the grain boundaries between the alumina and YAG phases. Qualitatively, the $PrAlO_4$ addition appeared to produce more crack deflection than the $CeAl_{12}O_{19}$ phase.

EFG Solidification Studies

Based on the work done at Northwestern, the most promising two modifier systems, $PrAlO_4$ and $CeAl_{12}O_{19}$ modified YAE, as well as the baseline YAE were grown by the EFG process. Approximately 5 wt% $PrAlO_4$ or $CeAl_{12}O_{19}$ modifier were added to the runs which contained modifiers. The YAE and the $PrAlO_4$ modified YAE were grown both in rectangular (31.75 mm x 4.83 mm) and rod (75 μm and 5 mm) cross-sections while the $CeAl_{12}O_{19}$ modified YAE was grown in rod form. The unmodified YAE was slightly pink in color, the praseodymium was green in color, and the cesium was bright yellow in color. There was some cracking present in the unmodified and praseodymium modified YAE rectangular cross-section materials, most likely due to a large thermal gradient in the ribbon due to a less than optimum insulation configuration. The 5 mm rod eutectic growth runs also showed some evidence of cracking, possibly due to the thermal mismatch between the molybdenum seed and the eutectic material, as all of the cracking was present at or near the seed junction and did not propagate down the length of the rod. The cracking was not a great concern, as the intent here was to investigate the microscopic and not macroscopic properties. Samples of the modified and unmodified YAE ribbons and rods were sent to Northwestern for microstructural evaluation.

The most promising composition, the $PrAlO_4$ modified YAE melt, was also grown as a 75μm fiber. One growth run, YII-042, which had a modifier level of ~0.3 wt%, had a mean room temperature tensile strength of 1.2 GPa (175 Ksi) with a standard deviation of 0.35 GPa (31 Ksi). This value was disappointing when compared to the YAE baseline fiber which had a room temperature tensile strength of ~2.1 GPa (300 Ksi). It is possible that this would be

increased with better optimization of the modifier level which was not possible due to the time constraints of this program.

Conclusions:

It was demonstrated that reproducible growth of YAE 75μm fiber is possible with the EFG process. The most promising growth parameter for growth rate was determined with a value of 0.6 in/min (0.25 mm/sec). This value was a compromise between tensile strength and growth stability. The growth of large numbers of fibers (>10) at once was very difficult for long periods of time. The reasons identified for this were: an increased sensitivity of the 75μm YAE fiber to perturbations in the growth rate and temperature as compared to the 150μm YAE fiber, a thermal gradient between the die tips, and melt level effects. The design of a large setup was completed but due to the issues with growing multiple fibers was not purchased as additional effort was spent on increasing the number of fibers growing at once.

A significant effort was made to determine the most suitable modifiers with which to weaken the interface in the eutectic microstructure so as to increase the toughness of the material. It was determined by Northwestern University that both the $PrAlO_4$ and $CeAl_{12}O_{19}$ phases produced significant crack deflection at the phase boundaries. Of the two materials the $PrAlO_4$ phase appeared to be more efficacious in producing a tough microstructure. When combined with the work done at NASA Lewis on the off-eutectic YAG-alumina compositions, it is expected that with slightly more investigation the optimum YAE modified fiber would be produced.

Table I - Run Summary						
Run ID	Date Grown	Pull Rate (in/min)	Length Grown m (ft)	# of Fibers	Modifier (wt%)	Comments
YAEII001	10/4/96	0.6-1.0	26 (85)	22	---	Seed Fibers
YAEII002	10/8/96	0.75	5 (17)	14	---	
YAEII003	10/23/96	0.80	7.3 (24)	7	---	
YAEII004	10/30/96	0.80	32 (107)	11	---	
YAEII005	11/2/96	0.80	~24 (80)	8	---	
YAEII006	11/8/96	0.80	93 (307)	2	---	
YAEII007	11/21/96	0.80	----	----	---	Die not feeding
YAEII008	7/16/97	0.30	0.7 (2.3)	1	---	Broke at seed junction
YAEII009	7/15/97	0.50	1.2 (4)	1	---	Fiber kinked
YAEII010	7/22/97	0.50	4.5 (14.6)	1	---	
YAEII011	7/24/97	0.50	0.7 (2.4)	1	---	
YAEII012	7/28/97	-----	-----	----	---	Setup blobbed
YAEII013	7/31/97	0.52	1.5 (4.9)	3	---	
YAEII014	8/7/97	0.50	63 (207)	1	---	
YAEII015	8/18/97	0.60	1.3 (4.4)	1	---	
YAEII016	8/26/97	0.76	1.5 (4.89)	3	---	
YAEII017	9/4/97	0.62	3.6 (11.8)	1	---	
YAEII018	9/5/97	0.65	45 (149)	4	---	
YAEII019	6/24/98	0.50	6.4 (21)	1	---	
YAEII020	6/25/98	0.45	4.8 (15.8)	2	---	
YAEII021	6/26/98	0.50	3.3 (10.9)	1	---	
YAEII022	6/29/98	0.55	15.7 (51.7)	3	---	
YAEII023	7/2/98	0.65	5.2 (16.9)	1	---	
YAEII024	7/3/98	0.25	3.4 (11.2)	1	---	
YAEII025	7/24/98	0.65	2.3 (7.5)	1	---	
YAEII026	7/28/98	0.60	39.3 (129)	1	---	

YAEII027	8/04/98	0.016	0.063	1	---	YAE Ribbon
YAEII028	8/05/98	0.012	0.028	1	---	YAE Ribbon
YAEII029	8/05/98	0.012	0.042	1	---	YAE Ribbon
YAEII030	8/06/98	0.016	0.125	1	---	YAE Ribbon
YAEII031	8/10/98	0.0125	0.472	1	1	YAE/Pr_2O_3 Rod
YAEII032	8/13/98	0.016-0.07	0.5 (0.152)	1	1	YAE/Pr_2O_3 Rod
YAEII033	8/14/98	0.016-0.032	1.0 (0.305)	1	1	YAE/Pr_2O_3 Rod
YAEII034	8/17/98	0.016-0.064	0.1 (0.229)	1	1	YAE/Pr_2O_3 Rod
YAEII035	8/18/98	0.016-0.075	0.75 (0.229)	1	<1	YAE/Pr_2O_3 Rod
YAEII036	8/19/98	0.016-0.065	0.67 (0.203)	1	---	YAE Rod
YAEII037	8/19/98	0.016	0.617	1		YAE/CeO_2 Rod
YAEII038	8/20/98	0.016-0.032	0.292	1		YAE/CeO_2 Rod
YAEII039	8/21/98	0.02-0.05	0.583	1		YAE/CeO_2 Rod
YAEII040	8/24/98	0.1-0.4	6.08 (1.854)	1		YAE/Pr_2O_3 Fiber
YAEII041	8/25/98	0.1-0.4	--	2		YAE/Pr_2O_3 Fiber
YAEII042	8/25/98	0.55	10.8 (3.302)	1		YAE/Pr_2O_3 Fiber
YAEII043	8/26/98	0.55	22.9 (6.985)	1		YAE/Pr_2O_3 Fiber
YAEII044	8/27/98	0.064	--	1		YAE/Pr_2O_3 Ribbon
YAEII045	8/27/98	0.032	--	1		YAE/Pr_2O_3 Ribbon

Table II. Tensile Test Data Run YAEII-003 Room Temperature Data						
Sample #	ID	Load	Avg. Dia. (mm)	Strength GPa/Ksi		Comments
1	38-18-3	362	70.1	1.84	267	End Failure
2	38-3-1	506	71.0	2.51	364	
3	38-8-2	308	70.2	1.75	254	
4	38-28-4	436	72.1	2.10	305	
5	38-3-3	351	71.2	1.73	251	
6	38-23-1	269	70.5	1.35	196	
7	38-18-2	421	70.2	2.13	309	
8	38-23-2	334	70.6	1.67	242	End Failure
9	38-23-3	423	71.1	2.09	303	
10	38-8-1	356	72.1	1.71	248	
11	38-3-4	381	71.7	1.85	268	
12	38-18-1	360	70.7	1.80	261	
13	38-8-4	286	71.0	1.42	206	
14	38-3-2	330	71.3	1.62	235	
15	38-23-4	309	70.8	1.54	223	
16	38-18-4	336	70.6	1.68	244	
17	38-28-3	375	72.1	1.80	261	
18	38-8-3	351	71.9	1.70	247	
19	38-28-2	448	71.1	2.18	316	
20	38-28-1	414	71.7	2.01	291	
Average				1.82	264	
Standard Deviation				0.28	40	

Table III. Tensile Test Data Run YAEII-004 Room Temperature Data						
Sample #	ID	Load	Avg. Dia. (mm)	Strength GPa/Ksi		Comments
1	32-38-2	345	62.3	2.22	322	End failure
2	32-3-4	367	66.6	2.07	300	End failure
3	32-38-3	----	65.0	----	----	Broke on set up
4	32-48-2	350	65.4	2.04	296	
5	32-23-2	373	63.0	2.35	341	
6	32-23-4	284	62.6	1.81	262	
7	32-13-1	303	63.6	1.87	271	End Failure
8	32-38-4	347	64.0	2.12	307	
9	32-13-2	214	64.4	1.29	187	
10	32-23-3	280	62.6	1.78	258	
11	32-23-1	371	64.0	2.26	328	
12	32-3-2	404	66.5	2.28	331	
13	32-3-1	348	66.1	1.99	289	
14	32-38-1	256	64.7	1.53	222	
15	32-48-4	293	64.7	1.75	254	
16	32-48-3	317	65.5	1.85	268	
17	32-13-4	192	64.7	1.15	167	
18	32-3-3	366	66.8	2.05	297	
19	32-13-3	286	63.7	1.76	255	
20	32-48-1	255	65.6	1.48	215	
Average				1.88	272	
Standard Deviation				0.33	48	

Table IV. Tensile Test Data Run YAEII-006 Room Temperature Data						
Sample #	ID	Load	Avg. Dia. (mm)	Strength GPa/Ksi		Comments
1	32-66-1	420	71.6	2.05	297	End failure
2	32-11-1	331	72.7	1.56	226	End failure
3	32-66-4	----	71.6	-----	----	Broke on set up
4	32-66-2	570	72.1	2.74	397	End failure
5	32-11-3	428	72.4	2.04	296	
6	32-71-1	484	71.8	2.35	341	
7	32-71-3	356	72.1	1.71	248	End failure
8	32-11-2	416	72.3	1.99	289	
9	32-66-3	374	71.8	1.81	262	
10	32-1-4	347	74.9	1.55	225	
11	32-71.4	170	70.6	0.85	123	
12	32-71.2	494	72.9	2.32	336	
13	32-16-2	434	72.5	2.06	299	
14	32-1-3	399	74.4	1.80	261	
15	32-16-1	291	71.5	1.42	206	
16	32-11-4	213	71.1	1.05	152	
17	32-1-2	409	76.2	1.76	255	
18	32-1-1	469	74.2	2.13	309	
19	32-16-3	366	71.7	1.78	258	
20	32-16-4	380	72.2	1.82	264	
Average				1.78	258	
Standard Deviation				0.39	57	

Table V. Tensile Test Data Run YAEII-019 Room Temperature Data						
Sample #	ID	Load	Avg. Dia. (mm)	Strength GPa/Ksi		Comments
1	1-1	422	75	1.91	277	
2	1-2	325	80.1	1.29	187	
3	1-3	--	81.4	--		Broke on setup
4	1-4	303	77.4	1.29	187	
5	1-5	353	74.7	1.61	234	
6	1-6	147	77.8	0.62	90	
7	1-7	--	73.6	--		Broke on setup
8	1-8	--	74.8	--		End failure
9	1-9	368	75.4	1.65	239	
10	2-1	391	73.6	1.84	267	
11	2-2	423	74.5	1.94	281	
12	2-3	209	76.9	0.90	131	
13	2-4	418	73.3	1.98	287	
14	2-5	394	74.7	1.80	261	
15	2-6	397	76.9	1.71	248	
16	2-7	242	75.9	1.07	155	
17	2-8	450	75.5	2.01	192	
Average				1.54	244	
Standard Deviation				.44	64	

Table VI. Tensile Test Data Run YAEII-020A Room Temperature Data						
Sample #	ID	Load	Avg. Dia. (μm)	Strength GPa/Ksi		Comments
1	1-1	615	82.9	2.28	331	
2	1-2	446	81.7	1.70	247	
3	1-3	455	86.7	1.54	223	
4	1-4	358	81.9	1.36	197	
5	1-5	423	88.7	1.37	199	
6	1-6	398	86.6	1.35	196	
7	1-7	422	87	1.42	206	
8	1-8	471	77.8	1.98	287	
9	1-9	357	87.8	1.18	171	
10	1-10	432	82.4	1.62	235	
11	1-11	419	80.9	1.63	236	
12	1-12	369	82.5	1.38	200	
13	1-13	508	81	1.97	286	
14	1-14	--	92.9	--		End failure
15	1-15	466	81.2	1.80	261	
16	1-16	420	81.8	1.60	232	
17	1-17	395	82.2	1.49	216	
18	1-18	297	87.4	0.99	144	
19	1-19	484	83.7	1.76	255	
20	1-20	473	82	1.79	260	
Average				1.59	231	
Standard Deviation				0.30	44	

Table VII. Tensile Test Data Run YAEII-020B Room Temperature Data						
Sample #	ID	Load	Avg. Dia. (μm)	Strength GPa/Ksi		Comments
1	1-1	483	86.3	1.65	239	
2	1-2	465	83.7	1.69	245	
3	1-3	453	82.6	1.69	245	
4	1-4	512	82	1.94	281	
5	1-5	321	74.3	1.48	215	
6	1-6	386	86	1.33	193	
7	1-7	423	81.3	1.63	236	
8	1-8	433	80.1	1.72	249	
9	1-9	468	84.7	1.66	241	
10	1-10	395	82.4	1.48	215	
11	1-11	474	81.7	1.81	263	
12	1-12	396	79.6	1.59	231	
13	1-13	263	66.1	1.53	222	
14	1-14	493	87.5	1.64	238	
15	1-15	479	86.8	1.62	235	
16	1-16	524	85.4	1.83	265	
17	1-17	485	83.1	1.79	260	
18	1-18	515	84	1.86	270	
19	1-19	490	84.9	1.73	251	
20	1-20	531	83.9	1.92	278	
Average				1.68	244	
Standard Deviation				0.16	23	

Table VIII. Tensile Test Data Run YAEII-021 Room Temperature Data						
Sample #	ID	Load	Avg. Dia. (μm)	Strength GPa/Ksi		Comments
1	1-1	401	55.8	3.28	476	
2	1-2	383	58	2.90	421	
3	1-3	257	62	1.70	247	
4	1-4	278	56	2.26	328	
5	1-5	258	58.1	1.95	283	
6	1-6	270	59.5	1.94	281	
7	1-7	265	57.2	2.06	299	
8	1-8	249	56	2.02	293	
9	1-9	249	55.4	2.07	300	
10	1-10	251	59.7	1.79	260	
11	1-11	283	59	2.07	300	
12	1-12	270	64	1.68	244	
13	1-13	298	59.7	2.13	309	
14	1-14	231	58.8	1.70	247	
15	1-15	203	54.3	1.75	254	
16	1-16	279	58	2.11	306	
17	1-17	286	59.6	2.05	297	
18	1-18	250	58.3	1.87	271	
19	1-19	288	65.9	1.69	245	
Average				2.05	297	
Standard Deviation				0.41	59	

Table IX. Tensile Test Data Run YAEII-022A Room Temperature Data						
Sample #	ID	Load	Avg. Dia. (μm)	Strength GPa/Ksi		Comments
1	1-1	721	82.9	2.67	387	
2	1-2	627	85.8	2.17	315	
3	1-3	622	84.1	2.24	325	
4	1-4	714	82.7	2.66	386	
5	1-5	421	86.3	1.44	209	
6	1-6	728	80.5	2.86	415	
7	1-7	646	82.8	2.40	348	
8	2-1	680	81.9	2.58	374	
9	2-2	486	85.1	1.71	248	
10	2-3	633	86.4	2.16	313	
11	2-4	659	84.5	2.35	341	
12	2-5	611	80	2.43	352	
13	2-6	659	82.6	2.46	357	
14	2-7	563	79.3	2.28	331	
15	3-1	403	86.9	1.36	197	
16	3-2	--	88.9	--	--	End Failure
17	3-3	472	86.1	1.62	235	
18	3-4	482	83.5	1.76	255	
19	3-5	497	82.9	1.84	367	
20	3-6	479	86.2	1.64	238	
21	3-7	408	86.1	1.40	203	
Average				2.10	305	
Standard Deviation				0.47	59	

Table X. Tensile Test Data Run YAEII-022B Room Temperature Data						
Sample #	ID	Load	Avg. Dia. (μm)	Strength GPa/Ksi		Comments
1	1	494	77	2.12	307	
2	1	449	81.8	1.71	248	
3	1	492	76	2.17	315	
4	1	518	80.4	2.04	296	
5	1	485	78.6	2.00	290	
6	1	519	83.4	1.90	276	
7	1	469	78.9	1.92	278	
8	2	257	74.5	1.18	171	
9	2	440	80	1.75	254	
10	2	353	75.2	1.59	231	
11	2	486	81.8	1.85	268	
12	2	550	78.4	2.28	331	
13	2	327	73.5	1.54	223	
14	2	378	78.8	1.55	225	
15	3	482	82.6	1.80	261	
16	3	468	80.5	1.84	267	
17	3	452	80.2	1.79	260	
18	3	501	80.3	1.98	287	
19	3	445	80	1.77	257	
20	3	403	71.8	1.99	289	
21	3	462	80.4	1.82	264	
Average				1.84	267	
Standard Deviation				0.25	36	

Table XI. Tensile Test Data Run YAEII-022C Room Temperature Data						
Sample #	ID	Load	Avg. Dia. (μm)	Strength GPa/Ksi		Comments
1	1-1	455	73.1	2.17	315	
2	1-2	441	74.2	2.04	296	
3	1-3	338	76.3	1.48	215	
4	1-4	425	73.6	2.00	290	
5	1-5	428	75.9	1.89	274	
6	1-6	482	78.9	1.97	286	
7	1-7	467	79.5	1.88	273	
8	1-8	442	76.8	1.91	277	
9	2-1	430	76.3	1.88	273	
10	2-2	459	77.2	1.96	284	
11	2-3	466	77	2.00	290	
12	2-4	437	81.6	1.67	242	
13	2-5	321	74.3	1.48	215	
14	2-6	448	74.8	2.04	296	
15	2-7	471	80.5	1.85	268	
16	3-1	502	81	1.95	283	
17	3-2	485	79.6	1.95	283	
18	3-3	511	80.3	2.02	293	
19	3-4	351	73.4	1.66	241	
20	3-5	460	82.3	1.73	251	
21	3-6	430	81.2	1.66	241	
22	3-7	399	78.2	1.66	241	
Average				1.86	270	
Standard Deviation				0.19	28	

Table XII. Tensile Test Data Run YAEII-023 Room Temperature Data						
Sample #	ID	Load	Avg. Dia. (μm)	Strength GPa/Ksi		Comments
1	1-1	632	79.6	2.54	368	
2	1-2	332	68.3	1.81	262	
3	1-3	409	77.8	1.72	249	
4	1-4	757	79.5	3.05	442	
5	1-5	669	80.8	2.61	378	
6	1-6	346	67.7	1.92	278	
7	1-7	--	65	--	--	End Failure
8	1-8	286	65.8	1.68	244	
9	1-9	461	74.1	2.14	310	
10	1-10	666	79.4	2.69	390	
11	1-11	668	78.8	2.74	397	
12	1-12	269	65.2	1.61	234	
13	1-13	462	78.9	1.89	274	
14	1-14	623	80.5	2.45	355	
15	1-15	461	76.8	1.99	289	
16	1-16	586	81.8	2.23	332	
17	1-17	576	78	2.41	350	
18	1-18	511	77.6	2.16	313	
19	1-19	479	73.8	2.24	325	
20	1-20	415	75.2	1.87	277	
Average				2.20	319	
Standard Deviation				0.41	60	

Table XIII. Tensile Test Data Run YAEII-024 Room Temperature Data						
Sample #	ID	Load	Avg. Dia. (μm)	Strength GPa/Ksi		Comments
1	1-1	401	70.9	2.03	294	
2	1-2	329	69	1.76	255	
3	1-3	287	69.3	1.52	220	
4	1-4	248	75.7	1.10	160	
5	1-5	479	74.1	2.22	322	
6	1-6	474	76.2	2.08	302	
7	1-7	499	74.8	2.27	329	
8	1-8	555	72.9	2.66	386	
9	1-9	521	74.8	2.37	344	
10	1-10	533	72.1	2.61	378	
11	1-11	603	71.9	2.97	430	
12	1-12	460	67.1	2.60	377	
13	1-13	429	74.5	1.97	286	
14	1-14	520	66.9	2.96	429	
15	1-15	591	76.2	2.59	376	
16	1-16	373	67.7	2.07	300	
17	1-17	401	63	2.57	373	
18	1-18	600	73.9	2.80	406	
19	1-19	393	63	2.52	365	
20	1-20	666	71.7	3.30	479	
Average				2.35	341	
Standard Deviation				0.53	77	

Table XIV. Tensile Test Data Run YAEII-025 Room Temperature Data						
Sample #	ID	Load	Avg. Dia. (μm)	Strength GPa/Ksi		Comments
1	1	722	91.4	2.20	319	
2	1	799	81	3.10	450	
3	1	691	81	2.68	402	
4	1	--	83.5	--	--	
5	1	873	92.3	2.61	379	
6	1	770	81.8	2.93	425	
7	1	676	84.5	2.41	350	
8	1	542	86.6	1.84	267	
9	1	999	82.8	3.71	538	
10	1	807	80.9	3.14	455	
11	1	597	85.1	2.10	305	
12	1	802	90.2	2.51	364	
13	1	884	88.7	2.86	415	
14	1	642	80.1	2.55	370	
15	1	933	92.6	2.77	402	
16	1	888	91.2	2.72	394	
17	1	853	91.4	2.60	377	
18	1	605	90.5	1.88	273	
19	1	599	81.1	2.32	336	
20	1	919	92.4	2.74	397	
Average				2.61	379	
Standard Deviation				0.45	65	

Table XV. Tensile Test Data Run YAEII-026A Room Temperature Data						
Sample #	ID	Load	Avg. Dia. (μm)	Strength GPa/Ksi		Comments
1	1	580	92.1	1.74	252	
2	1	519	92	1.56	226	
3	1	603	93.4	1.76	255	
4	1	542	90.9	1.67	242	
5	1	624	93.2	1.83	265	
6	1	443	92.1	1.33	193	
7	1	621	93.7	1.80	261	
8	1	520	91	1.60	232	
9	1	569	91.5	1.73	251	
10	1	588	90	1.85	268	
11	2	528	91.1	1.62	235	
12	2	563	92.1	1.69	245	
13	2	451	91.9	1.36	197	
14	2	596	93.4	1.74	252	
15	2	572	94.8	1.62	235	
16	2	788	92	2.37	235	
17	2	840	96.2	2.31	335	
18	2	877	98.1	2.32	336	
19	2	867	95.7	2.41	350	
20	2	875	94.6	2.49	361	
21	3	847	96.2	2.33	338	
22	3	933	97.5	2.50	362	
23	3	796	91.5	2.42	351	
24	3	839	93	2.47	358	
25	3	838	93.7	2.43	352	
26	3	837	91.8	2.53	367	
27	3	883	92.3	2.64	383	
28	3	826	93.6	2.40	348	
29	3	762	93.1	2.24	348	
30	4	902	94.9	2.55	370	
31	4	782	91.3	2.39	347	
32	4	911	95.4	2.55	370	
33	4	823	91.9	2.48	359	
34	4	888	94.9	2.51	364	
35	4	817	89.8	2.58	374	

36	4	940	95.6	2.62	380	
37	4	790	89.7	2.50	362	
38	4	790	91	2.43	352	
Average				2.14	310	
Standard Deviation				0.41	59	

Table XVI. Tensile Test Data

Run YAEII-26B Room Temperature Data

Sample #	ID	Load	Avg. Dia. (μm)	Strength GPa/Ksi		Comments
1	1-1	--	61.9	--	--	Failed Test
2	1-2	455	58.4	3.40	493	
3	1-3	--	57.8	--	--	Failed Test
4	1-4	359	55.4	2.98	432	
5	1-5	--	58.6	--	--	Failed Test
6	1-6	464	54.6	3.96	574	
7	1-7	432	56.3	3.47	503	
8	1-8	471	58.9	3.46	502	
9	1-9	--	59.6	--	--	Failed Test
10	1-10	434	53.3	3.89	564	
11	1-11	282	58.9	2.07	300	
12	1-12	224	59.4	1.62	235	
13	1-13	262	57.0	2.05	297	
14	1-14	240	57.5	1.85	268	
15	1-15	276	57.6	2.12	307	
16	1-16	301	57.5	2.32	336	
17	1-17	266	58.3	1.99	289	
18	1-18	257	59.6	1.84	267	
Average				2.64	383	
Standard Deviation				0.84	122	

Table XVII. Tensile Test Data Run YAEII-042 Room Temperature Data						
Sample #	ID	Load	Avg. Dia. (μm)	Strength GPa/Ksi		Comments
1	1-1	214	94.6	0.61	89	
2	1-2	--	94.7	--	--	End Failure
3	1-3	375	92.8	1.11	161	
4	1-4	488	92.3	1.46	212	
5	1-5	339	91.6	1.03	149	
6	1-6	--	94.7	--	--	End Failure
7	1-7	523	94.2	1.50	218	
8	1-8	365	90.7	1.13	164	
9	1-9	537	95.2	1.51	219	
10	1-10	488	91	1.50	218	
11	1-11	567	98.8	1.48	215	
12	1-12	394	93.8	1.14	165	
13	1-13	145	88.7	0.47	68	
14	1-14	632	97.9	1.68	244	
15	1-15	364	92.6	1.08	157	
16	1-16	396	92.4	1.18	171	
Average				1.21	175	
Standard Deviation				0.35	31	

Table XVIII - Doped YAE Eutectic X-Ray Phase Analysis		
Modifier	Phases	Comments
$NdAlO_4$	Corundum, YAG	Very small (3%) unidentified peaks remaining.
$PrAlO_4$	Corundum, YAG	Small (6%) unidentified peaks remaining.
$SrAl_{12}O_{19}$	Corundum, YAG, YAP, $SrAl_{12}O_{19}$	Not enough alumna added to melt, strontium scavenged alumina from YAG and produced YAP.
$CaAl_{12}O_{19}$	Corundum, YAG	Very small (3%) unidentified peaks remaining.
Ce $Al_{12}O_{19}$	Corundum, YAG	Very small (4%) unidentified peaks remaining.
$LaAlO_4$	Corundum, YAG	Large (35%) unidentified peaks remaining.
$LaTaO_4$	Corundum, YAP	Undesirable YAP phase present.
$YTaO_4$	Corundum, YAP	Undesirable YAP phase present.
$YNbO_4$	Corundum, YAP	Undesirable YAP phase present.
$CaWO_4$	Corundum, YAG, $CaWO_4$	Small (10%) unidentified peaks remaining.
$LaAlO_4$	Corundum, YAP	Undesirable YAP phase present.
TiO_2	Corundum, YAG	Wanted Al_2TiO_5, not clear whether it is present, need to do additional testing to determine if it is present.

[1] K. L. Luthra and H.D. Park, "Chemical Compatibility in Ceramic Composites," AFWAL-TR-89-6009.

[2] M.B. Boron , M.K. Brun and L.E. Szala, "Kinetics of Oxidation of Carbide and Silicide Dispersed Phaese in Oxide Matricies," Adv. Ceram. Mater., 3(5) 491-97.

[3] P. Shahinian, "High-Temperature Strength of Sapphire Filament," J. Am. Ceram. Soc., 54 (1) 67-68.

[4] L.E. Jones and R.E. Tressler, "The High Temperature Creep Behavior of Oxides and Oxide Fibers," NASA Contractor Report #187060, Jan. 1991.

[5] Private communication with Dr. Ali Sayir of NASA Lewis Research Center.

Appendix I

Nanostructural Analysis of Additive-Modified

YAG-Al_2O_3 Eutectics (YAE's)

by

Vinayak P. Dravid

Associate Professor, MS & E

Northwestern University, Evanston, IL 60208

Ph.: (847) 467-1363, Fax: (847) 491-7820

E-mail: v-dravid@nwu.edu

SUMMARY

Several "additive-modified" eutectics of YAG-Al_2O_3 were investigated using SEM and TEM analysis. It is shown that the general eutectic microstructure is retained with additives such as, $CaWO_4$, $CeAl_{11}O_{18}$, $CaAl_{12}O_{19}$ and $Pr_xAl_yO_z$. However, additives such as: $LaNbO_4$, $La_xAl_yO_z$, $LaTaO_4$, $YNbO_4$, $YTaO_4$ tend to destabilize the eutectic morphology. Subsequent TEM and microanalysis work on those containing additives which retain the eutectic microstructure show that preferred enrichment of $CaWO_4$, $CeAl_{11}O_{18}$ and $Pr_xAl_yO_z$ modifiers is possible for eutectic interfaces. $Pr_xAl_yO_z$, especially, displayed promising characteristics of consistent crack deflection at the eutectic interfaces. High resolution microanalysis clearly showed presence of Pr at these interfaces hinting towards the premise of weakening of eutectic interfaces by additives.

Although more detailed work is warranted on these systems, the results accomplished so far lend support to the premise that certain additives tend to favorably modify the interface bonding in YAG-Al_2O_3 eutectics and show indication of weakened bonding and promotion of crack deflection.

I. INTRODUCTION:

While YAG-Al_2O_3 directionally solidified eutectics (DSE's) possess excellent strength and creep resistance, the fracture toughness remains as the major concern for its future development in ceramic-matrix-composites (CMC's). One approach of possibly improving the fracture toughness is to make the DSE interfaces weak enough to allow a propagating crack to debond the interfaces and expend sufficient energy through a variety of mechanisms. One approach to "weaken" DSE interfaces is to introduce dopants/additives and alter either the bonding at DSE interfaces or introduce a ternary phase at DSE interfaces which itself would be weak in response to a propagating crack.

This report concentrates on SEM and TEM analysis of various additive-modified YAG-Al_2O_3 Eutectics (YAE's). The principal objectives for the analysis were to:

- Probe the microstructure at all length-scales (from several μm to <1 μm)
- Obtain evidence for the presence of the tertiary additives
- Conduct TEM imaging and microanalysis for detection of segregation to DSE interfaces.
- Conduct simple crack propagation trajectories in search for possible crack-deflection tendencies in some additive-modified YAE's.

The following additive-modified YAE's were investigated in our work.

$CaWO_4$ - YAE	$CeAl_{11}O_{18}$ - YAE	$CaAl_{12}O_{19}$ - YAE
$Pr_xAl_yO_z$ - YAE	$Nd_xAl_yO_z$ - YAE	$LaNbO_4$ - YAE
$La_xAl_yO_z$ – YAE	$LaTaO_4$ – YAE	$YNbO_4$ - YAE
$YTaO_4$ - YAE		

The approach of our undertaking was to examine the YAE sections using both SEM and TEM characterization. The efficacy of the additives in modifying the eutectic interface bonding was investigated indirectly by observing the crack propagation behavior after indentation.

bonding was investigated indirectly by observing the crack propagation behavior after indentation.

II. EXPERIMENTAL:

All the additive modified YAE's were prepared at Saphikon by melting and then rapidly cooling the nominal compositions in molybdenum crucibles. Cylindrical disk shaped melt solidified sections of various YAE's were cut into four quadrants. Both the faces and section edges were polished to optical quality using mechanical polishing and lapping, and viewed using optical microscopy and SEM for microstructure evaluation. Hitachi S4500-II cFEG SEM and Hitachi S570 cSEM were used to observe the microstructure. Some selected specimens were indented with Vickers diamond indenter to initiate cracking.

TEM specimen preparation involved sectioning disks to size of about 3 mm diameter. These disks were subsequently mechanically thinned to about 100 microns. Disks were further thinned using dimpler to be about 20-30 microns in the center. Gatan Ion Beam Thinner (IBT) was used to make electron transparent foils for TEM. TEM was performed using a Hitachi HF-2000 cFEG TEM/STEM, equipped with an Oxford x-ray detector and Gatan PEELS analyzer.

III. RESULTS AND DISCUSSION:

Based on conventional optical microscopy and SEM, Table I lists the general microstructural observations for all of the modified YAE's supplied:

Table I. Microstructural Observation in modified YAE melts.	
Phase	Comments
$CaWO_4$ - YAE	Eutectic structure is largely retained
$CeAl_{11}O_{18}$ - YAE	Eutectic structure is largely retained
$CaAl_{12}O_{19}$ - YAE	Eutectic structure is largely retained
$Pr_xAl_yO_z$ - YAE	Eutectic structure is largely retained
$Nd_xAl_yO_z$ - YAE	Eutectic structure is occasionally seen
$LaNbO_4$ - YAE	Eutectic structure is rarely seen
$La_xAl_yO_z$ - YAE	Eutectic structure is rarely seen
$LaTaO_4$ - YAE	Eutectic structure is rarely seen
$YNbO_4$ - YAE	Eutectic structure is rarely seen
$YTaO_4$ - YAE	Eutectic structure is rarely seen

Following these observations, we selected four YAE system for further SEM and TEM analysis. These were:

1) $CaWO_4$ - YAE Eutectic structure is largely retained.
2) $CaAl_{12}O_{19}$ - YAE Eutectic structure is largely retained.
3) $Pr_xAl_yO_z$ - YAE Eutectic structure is largely retained.
4) $CeAl_{11}O_{18}$ - YAE Eutectic structure is largely retained.

All of these specimens were subjected to indentation in search for crack propagation trajectories. What follows below is the summary for each of these materials systems.

1. $CaWO_4$ – YAE:

This DSE system exhibited the general eutectic morphology. SEM analysis did not show any obvious tertiary phase. Crack propagation studies showed some tendency for crack deflection at eutectic interfaces. Thus, we decided to make TEM specimen of this YAE in search for fine-scale segregation or presence of $CaWO_4$ rich phase at eutectic interfaces.

STEM imaging of TEM specimens, once again, did not exhibit any visible tertiary phase. There were several instances of "open" space at eutectic interfaces, indicative of some loss of material from such areas. However, STEM microanalysis clearly showed presence of W at various YAG-Al_2O_3 interfaces. Figure 1 is a STEM dark field image showing YAG-Al_2O_3 interface. A few "void looking" features are apparent in this image. STEM microanalysis profile across "intact" YAG-Al_2O_3 interface shows clear enrichment of W at the interface. Figure 2 shows such a STEM microchemistry plot. However, we did not observe presence of any Ca at these interfaces. It was concluded that Ca may have evaporated during growth process leaving behind W-rich eutectic interfaces.

2. $CaAl_{12}O_{19}$ – YAE:

In this system, it was hoped that Ca-aluminate may form a tertiary layered phase (hibonite) at YAG-Al_2O_3 interfaces. If so, then layered nature of the hibonite phase would likely lead to crack deflection. Unfortunately, the hibonite phase occurred as a distinct tertiary phase in pockets rather than at eutectic interfaces. Clearly, it doesn't appear to wet either of the interfaces. Crack propagation studies showed little or no crack deflection in accord with TEM studies. Figure 3 shows an SEM image of indentation on the eutectic structure. Note virtually no deflection at any interface in this YAE. No attempts were made to move onto TEM scale with this YAE

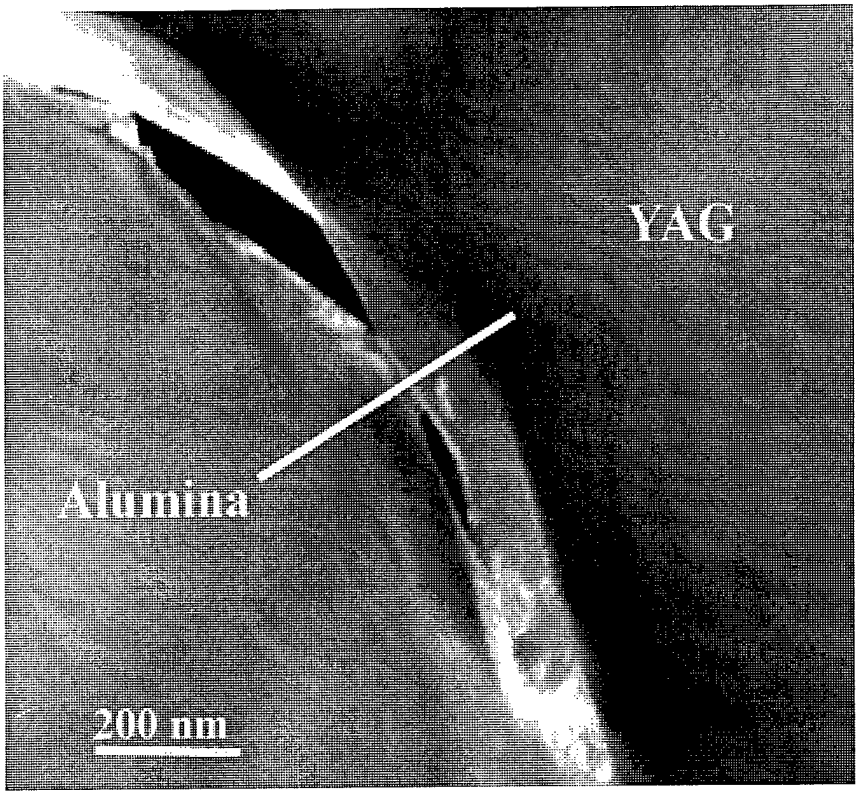

Figure 1. STEM dark field image of YAE interface.

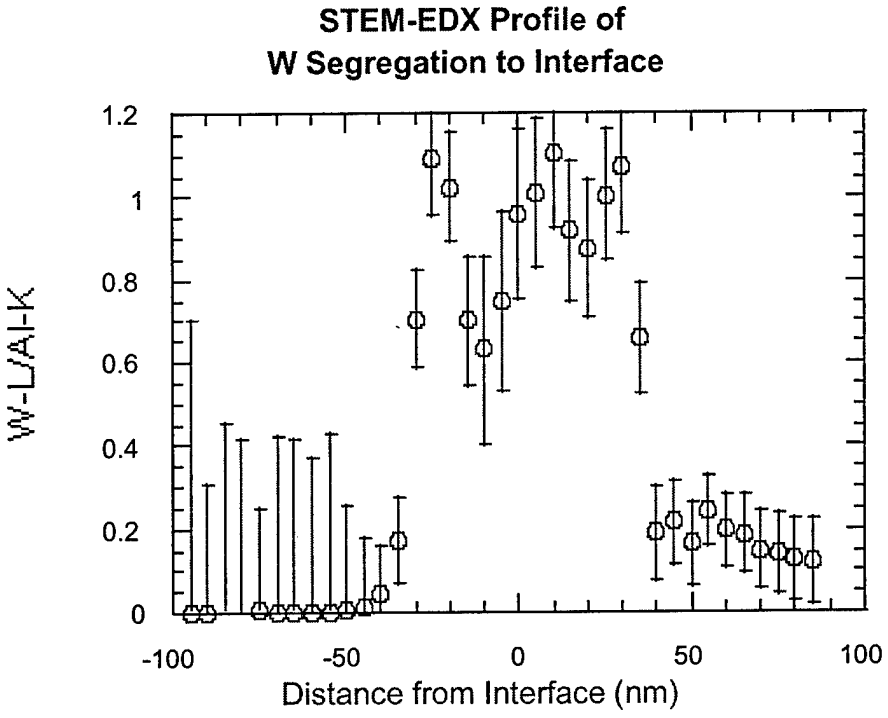

Figure 2. STEM microchemistry plot along line in Figure 1.

Figure 3. SEM image of indentation in Ca modified YAE.

3. $Pr_xAl_yO_z$ – YAE:

This system, by far, showed the most encouraging crack-propagation behavior. SEM images showed clear presence of Pr-rich aluminate at triple junction as well as at YAG-Al_2O_3 interfaces. Figure 4 shows a BSE image of this YAE indicating clear presence of Pr-rich phase at various location. Many cases of possible "wetting" of YAG-Al_2O_3 interfaces by Pr-rich phase was noted. Several instances of crack deflection at eutectic interfaces were noted in SEM studies. Figure 5 and 6 show BSE images of indented specimen. There is encouraging tendency of cracks to delaminate YAG-Al_2O_3 interfaces in some cases. It was decided to proceed to TEM analysis for such specimens.

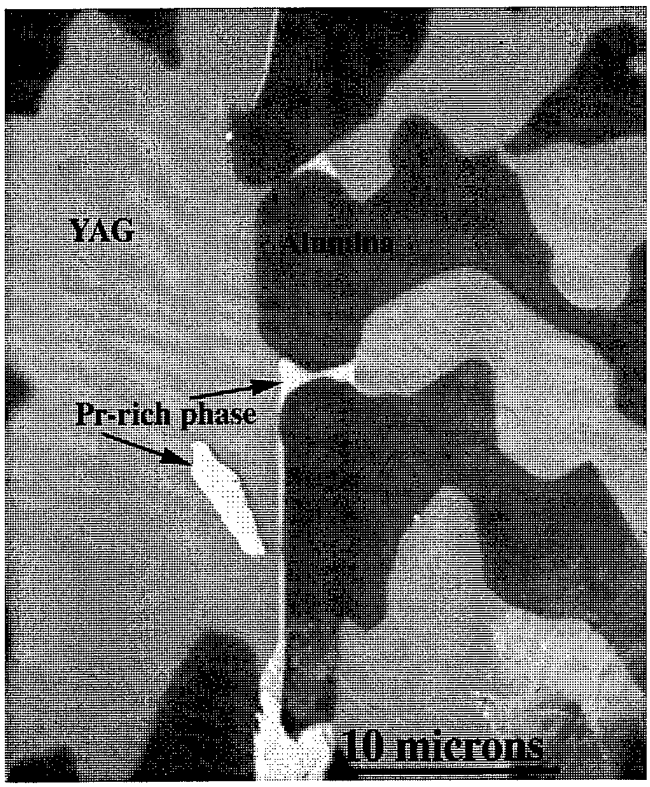

Figure 4. BSE image of Pr modified YAE

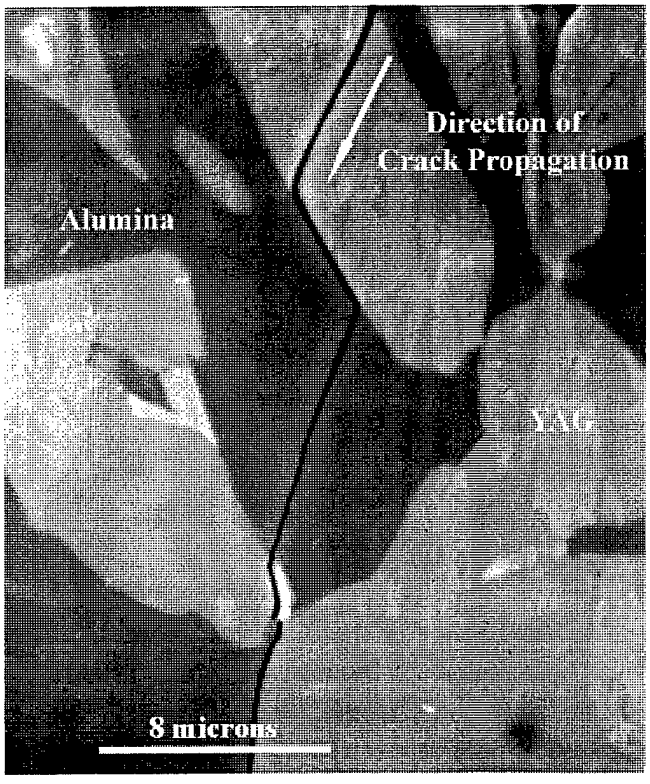

Figure 5. BSE image an indented sample of Pr modified YAE

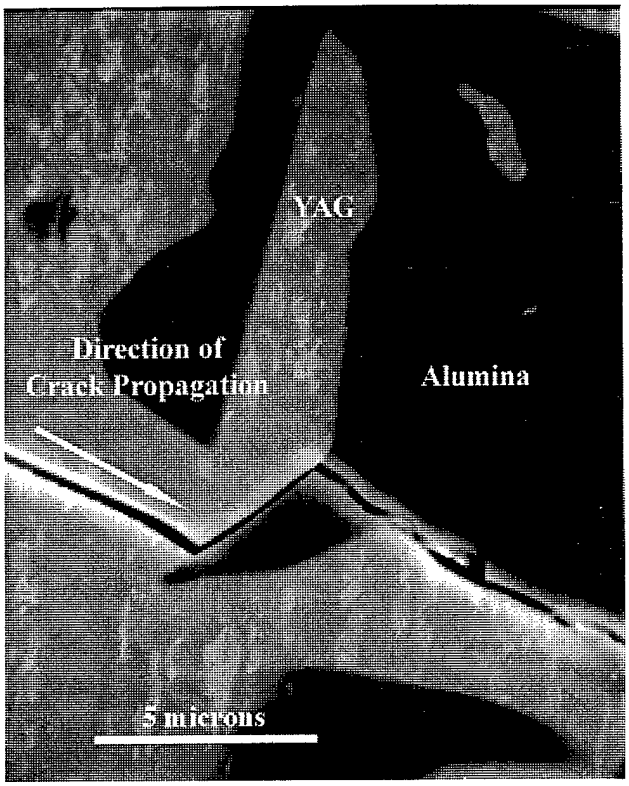

Figure 6. BSE image of indented Pr modified YAE.

TEM imaging showed clear presence of eutectic structure with a few isolated pockets of Pr-rich phase. The tendency of YAE modified with Pr for crack deflection was observed in TEM as well. Figure 7 shows a bright field TEM image of an accidental crack initiated in YAG phase. There is a clear deflection of this crack at the YAG-Al_2O_3 interface. Subsequent microanalysis at such interfaces showed clear evidence for Pr-enrichment at the interface. Figure 8 is a dark field STEM image of a YAG-Al_2O_3 interface, where the white line indicates the location of microanalysis profile. Note that there is no distinct tertiary phase at the interface. Microchemical profile shows clear presence of Pr enrichment at the interface (Figure 9). The Pr-enrichment is quite narrow, about less than 10 nm.

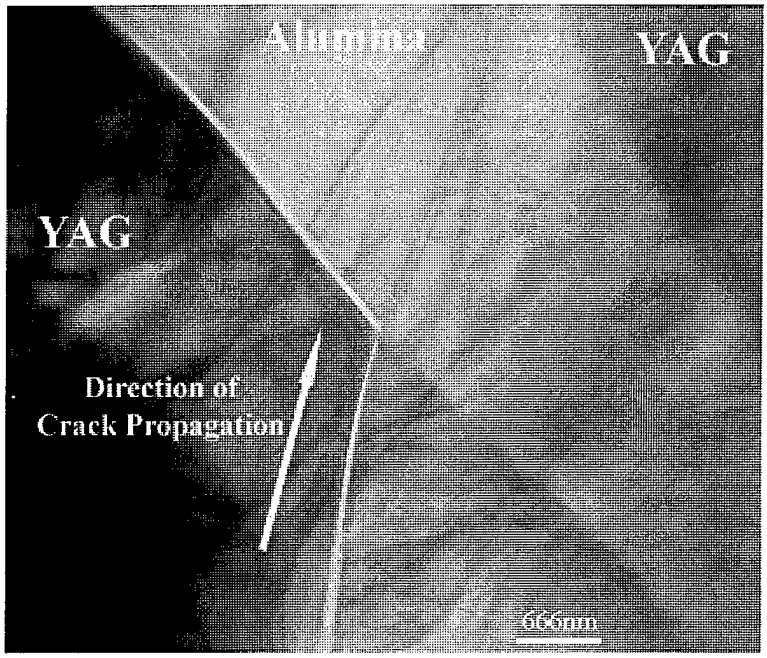

Figure 7. BF TEM image of crack in Pr modified YAE

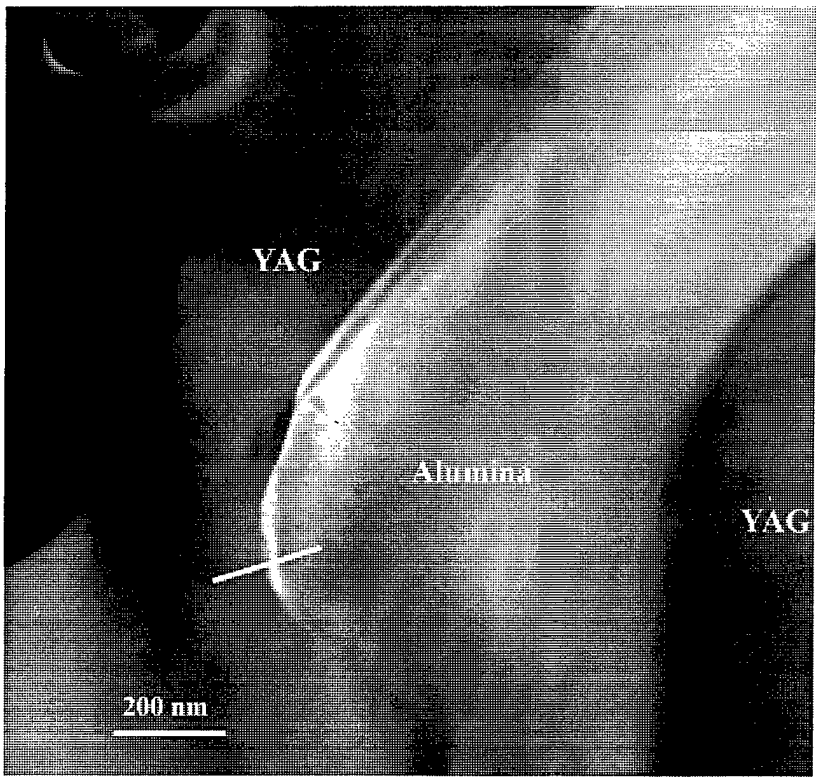

Figure 8. DF STEM image of Pr modified YAE.

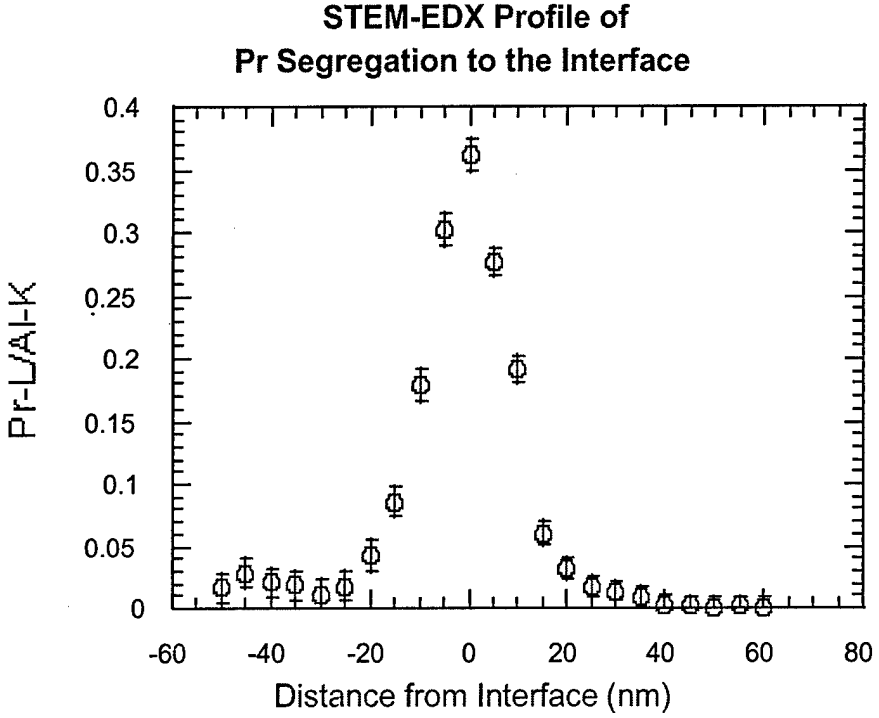

Figure 9. Microchemical profile of Pr modified YAE.

It was also noted that there is notable solubility of Pr in YAG phase itself. Figure 10 shows an EDS spectrum of YAG indicating notable Pr solubility. The Al_2O_3 phase, on the other hand, is completely devoid of any Pr, as indicated in spectrum in Figure 11.

Several TEM sessions were devoted to this system to obtain some degree to statistical confidence. On many occasions, Pr seems to be present as a segregant. On other occasions, a clear presence of thin tertiary phase rich in Pr was detected. This phase often decorated the YAG-Al_2O_3 interface and is assumed to be Pr-rich aluminate.

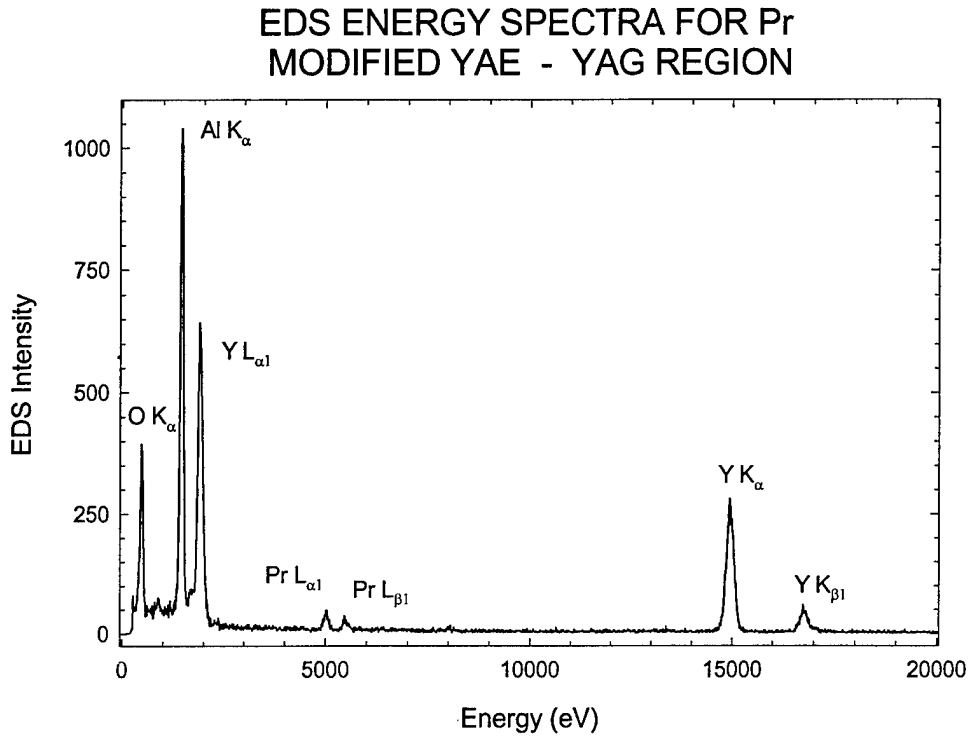

Figure 10. EDS spectra of Pr modified YAE - YAG region.

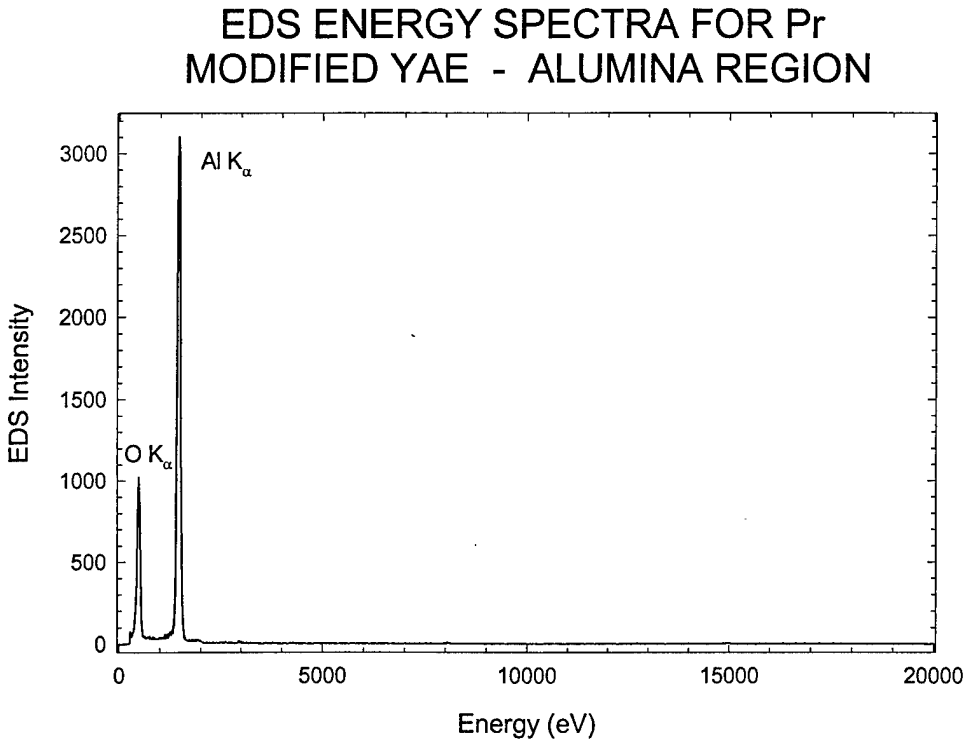

Figure 11. EDS spectra of Pr modified YAE - alumina region.

4. $CeAl_{11}O_{18}$ – YAE:

CeO_2-doped YAG-Al_2O_3 eutectic is expected to behave similar to CaO-doped systems, i.e. formation of $CeAl_{11}O_{18}$ phase which may facilitate crack deflection. On SEM scale, however, no clear presence of $CeAl_{11}O_{18}$ could be noted. The microstructure, though eutectic "looking", was often rather coarse. Crack propagation in response to indentation showed occasional crack deflection. There were some instances of crack following the YAG-Al_2O_3 interfaces, as in BSE image – Figure 12. TEM analysis, however, showed clear presence of Ce-rich phase at YAG-Al_2O_3 boundaries. Figure 13 is one such instance where there appears to be wetting of YAG-Al_2O_3 interface by $CeAl_{11}O_{18}$ –type phase.

Microchemical analysis of this phase is shown in Figure 14 EDS spectrum. Profuse enrichment of Ce-, in line with $CeAl_{11}O_{18}$ –type composition is seen. There is slight solubility of Ce in YAG (Figure 15), while there is virtually none in Al2O3 (Figure 16).

IV. CONCLUDING REMARKS:

In summary, considerable progress has been made towards the presence, identity and effect of tertiary dopants in YAG-Al_2O_3 DSE system. $Pr_xAl_yO_z$ doping by far showed the most promising results of both crack deflection as well as presence of Pr-rich interfaces and tertiary phase. While $CaWO_4$ showed crack deflection tendency, segregation was limited to only to W and Ca appears to be have been lost during melt-growth. Ca-doped YAE showed quite brittle behavior and presence of Ca-rich phase could not be confirmed. Ce-doped YAE showed clear presence of Ce-rich phase (most likely $CeAl_{11}O_{18}$) which appears to wet the YAG-Al_2O_3 interfaces. However, crack deflection tendency was noted to be rather occasional and weak.

Continued work on selectively doped YAG-Al_2O_3 directionally solidified eutectics should further shed light on the issue of segregation, tertiary phase formation and expected crack deflection in such controlled microstructures.

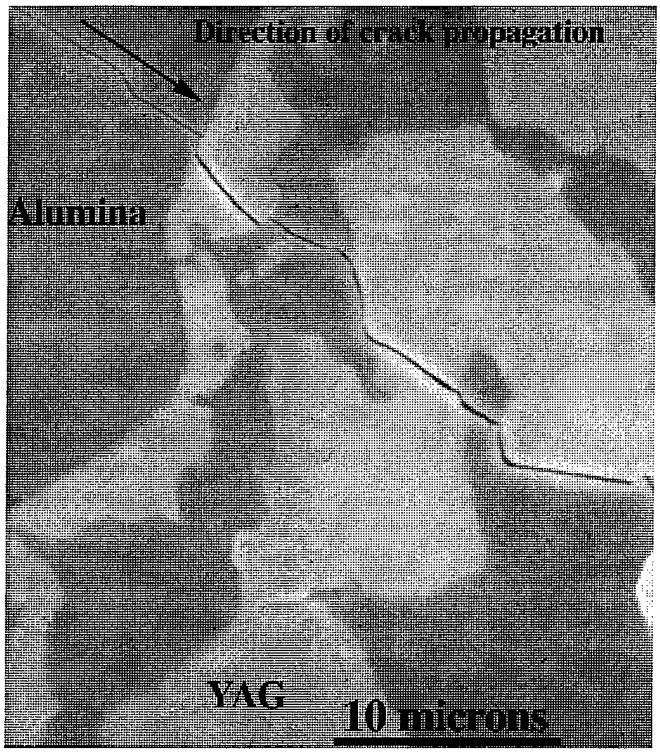

Figure 12. BSE image of Ce modified YAE.

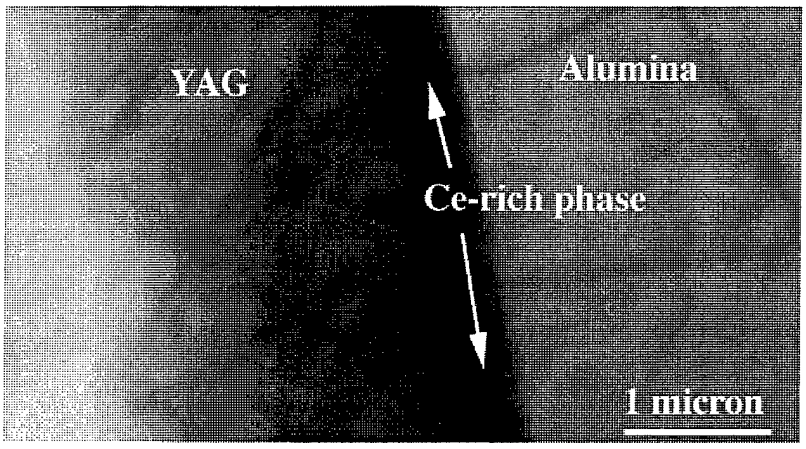

Figure 13. TEM image of Ce doped YAE.

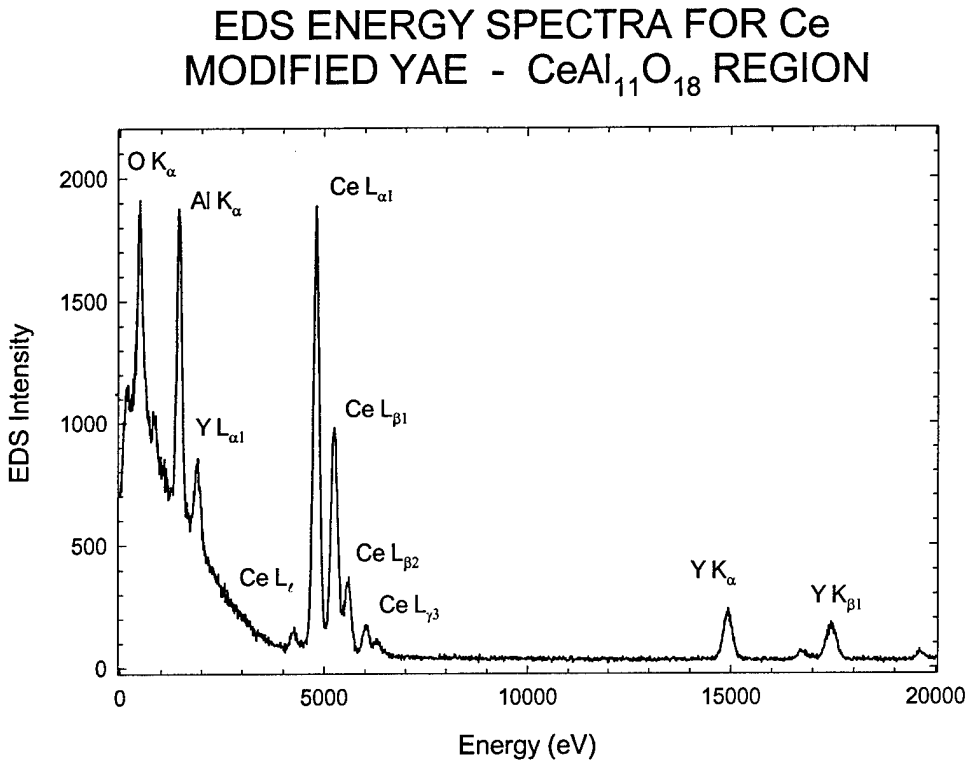

Figure 14. EDS spectra of Ce modified YAE - $CeAl_{11}O_{18}$ region.

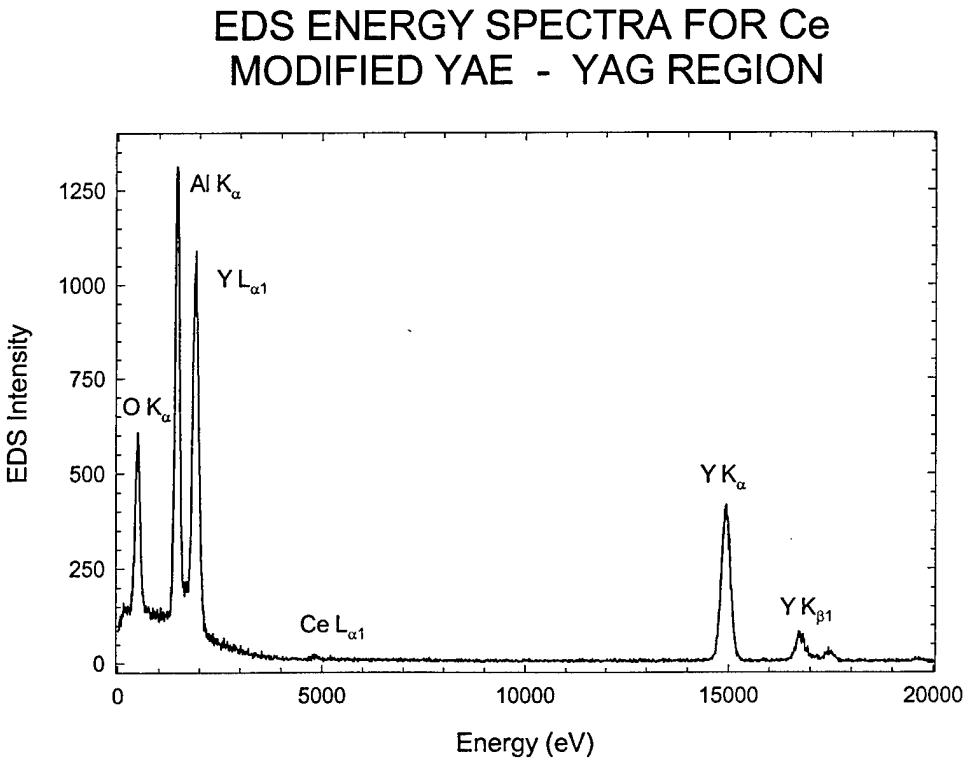

Figure 15. EDS spectra of Ce modified YAE - YAG region

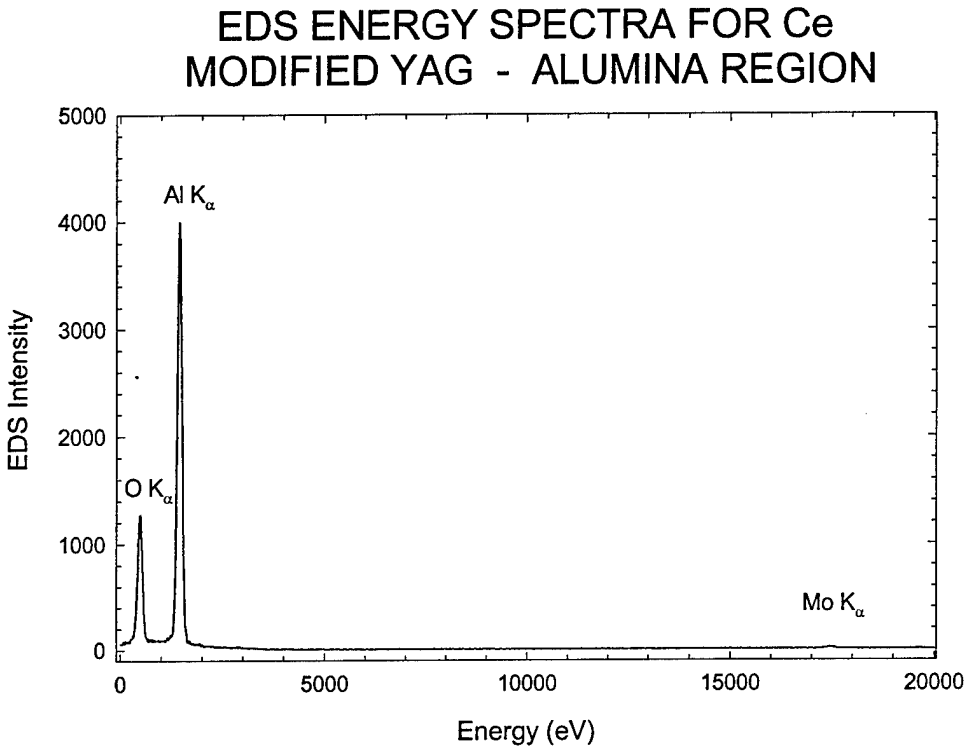

Figure 16. EDS spectra of Ce modified YAE - alumina region

APPENDIX II

A Study of the Off-Eutectic Growth Characteristics of Directionally Solidified $Al_2O_3/Al_3Y_5O_{12}$ (YAG) Fibers

Ali Sayir

Department of Materials Science and *Engineering*

Case Western Reserve University

Cleveland, OH 44106

ABSTRACT

The proposed research is to investigate two phase fibers made by eutectic directional solidification. A potential advantage of fibers containing fibrous eutectic microstructures is an effective reduction in reinforcement diameter, which is currently 100-250 μm for single crystal fibers. This program has two specific objectives that will be simultaneously pursued. These objectives are: (i) characterization of off-eutectic YAE fibers grown by way of the laser heated floating zone (LHFZ) process, and (ii) investigation of microstructural stability of off-eutectic compositions. The proposed work will be accomplished in two phases. The CO_2 laser-heated, floating-zone process (LHFZ) is currently being utilized for producing improved off-eutectic oxide fibers. The work concentrated on three principal tasks: (a) characterization of optimum off-eutectic compositions of (b) study of YAE fibers with textured, elongated grains and (c) high temperature mechanical studies of off-eutectic fibers.

I. BACKGROUND

• Introduction

Single crystal or precisely controlled polycrystalline oxide fibers grown from melts are among the likely candidates for reinforcement of high temperature ceramic, intermetallic and metal matrix composites due to their unique combination of thermal expansion coefficients, high temperature mechanical properties, and oxidation resistance. Oxide reinforcement materials previously investigated include pure and doped single crystals, columnar grained single phase materials, and polyphase materials (e. g. fibers grown from eutectic melts). Through deliberate selection of crystallographic growth axes and low dislocation mobilities, undamaged virgin fibers of several materials have exhibited test results that can be used to project uniaxial tensile creep rates that remain acceptable for temperatures up to approximately 1600°C.

The work described here, whose potential was foremost shown by Sayir and Matson,[1,2] is to investigate two phase fibers made by eutectic directional solidification. A potential advantage of fibers containing fibrous eutectic microstructures is an effective reduction in reinforcement diameter, which is currently 100-250 μm for single crystal fibers. Improved creep resistance is expected because it has been shown that reduction by a factor of ten in fiber diameter reduces creep rates by nearly two orders of magnitude. [3] Eutectic fibers offer a method of controlling the diameter of the reinforcement phase and to some extent the reinforcement distribution. Strength improvements are expected for the "in-situ composite fibers" because the matrix cracking stress has been shown to be inversely proportional to fiber diameter.[4] Initial attempts to produce an oriented eutectic microstructure with the LHFZ process were highly successful.

The eutectic architecture, a continuous reinforcing phase within a higher volume phase or matrix, can be described as a naturally occurring *in-situ* composite. In-situ composites demonstrate mechanical properties intermediate between monolithic materials and man-made composites. The phases comprising a eutectic are thermodynamically compatible at higher homologous temperatures than

man-made composites and as such offer the potential for superior high temperature properties.[5-8] The mechanical properties of two phase eutectics can be superior to that of either constituent alone due to strong constraining effects provided by the interlocking microstructure.

• Laser Heated Float Zone Growth (LHFZ)

In the laser-heated floating-zone (LHFZ) process, the melt is formed from heat absorbed by a focused CO_2 laser heat source and is supported by surface tension between the feed rod and the growing fiber. The LHFZ process is particularly suited to refractory fibers used in high temperature composites. Because the laser has no upper characteristic temperature limit, the beams can be focused to the dimensions needed for growth of small diameter fibers, and atmospheres can be selected freely to enhance the growth process, the fiber properties and the surface chemistry. An important advantage of the LHFZ process is its ability to produce fibers with different compositions free from interactions with crucibles or dies. The beneficial effects of dopants can be illustrated by the addition of specified dopants to off-eutectic compositions in short turn-over times and in a cost-effective manner. However, the LHFZ can grow only one fiber whereas the edge-defined film fed growth (EFG) process is capable of growing multiple fibers. Thus, compared with the EFG process the fiber growth with the LHFZ process is expensive for structural fibers.

• Objectives

This program had two specific objectives that were pursued simultaneously. These objectives are: (i) characterization of off-eutectic YAE fibers grown by the LHFZ process, and (ii) investigation of high temperature microstructural stability of directionally solidified YAE fibers.

(i) Fiber Development: The first objective will relate accessible growth properties to process variables of the reinforcements using LHFZ process. This first objective will define optimum fiber compositions having adequate properties. Reinforcement fibers having required properties must be produced at acceptable dimensions (diameter and lengths) and properties. To achieve these objectives, fiber quality, high temperature properties in oxidizing environments, and growth rates all must be improved simultaneously.

(ii) High Temperature Microstructural Characterization : This second objective will define the high temperature microstructural stability range for optimum fiber compositions and processing configurations.

The results are presented in reverse order. First, in Section 2, the time dependent characteristics of directionally solidified YAE eutectics will be discussed. Results on the relationships between lifetime, stress and temperature are presented. Second, in Section 3, the solidification characteristics of YAE off-eutectic liquids and the ramifications of melt characteristics in production of *in-situ* composite materials will be treated.

2. RESULTS AND DISCUSSION

2.1 MECHANICAL PROPERTIES

Laser heated float zone (LHFZ) was being used as a means to efficiently produce and record the underlying growth phenomena associated with two phase structures. Growth and characterization of single crystal and eutectic fibers are described in the literature[8,9] in detail and will be not be repeated here. Fibers grown either by LHFZ or EFG provided samples for research on the intrinsic mechanical properties of this class of materials.

2.1.1 High Temperature Strength - Slow Crack Growth and Creep

The fast fracture tensile strengths of as-received EFG fibers tested at 25 and 1100 °C are presented as Weibull probability plots in Fig. 1. A typical longitudinal surface morphology for YAE eutectic is shown in the Fig. 2. The room temperature tensile strength of YAE was 2.39 GPa, considerably lower than the tensile strength of c-axis sapphire, 3.2 GPa. However, the high temperature tensile strength of YAE eutectics is superior to sapphire, with YAE having a strength of 1.37 GPa and sapphire having a tensile strength of 1.1 GPa at 1100°C. To understand why YAE eutectic is stronger than sapphire at elevated temperature, it is necessary to consider how sapphire deforms. An independent study[10] showed that the failure of sapphire fibers is due to slow crack growth at T>1000°C. Two thermally activated mechanisms postulated to explain slow crack growth are atomistic level crack propagation due to lattice trapping, and/or dislocation assisted crack shielding.[11]

To assess the slow crack growth behavior of YAE, time dependent failure was first evaluated by examining the dependence of tensile strength on strain rate. The strain rate-dependent tensile strengths of directionally solidified YAE eutectic are compared with those of c-axis sapphire in Fig. 3. The tensile strength of the directionally solidified YAE did not vary with a change in strain rate spanning four orders of magnitude. The tensile strength of the eutectic fibers was 1.35 GPa at

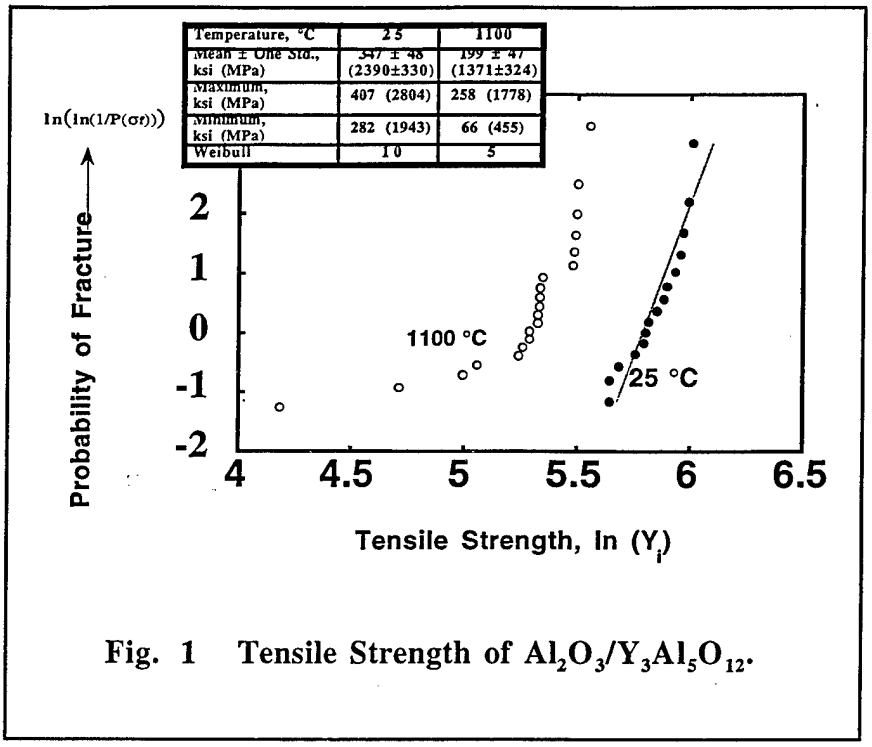

Fig. 1 Tensile Strength of $Al_2O_3/Y_3Al_5O_{12}$.

1100°C. Under similar test conditions, the tensile strength of c-axis sapphire showed a strong dependence on strain rate, Fig. 3. The resistance of YAE to slow crack growth is clearly superior to the resistance of sapphire alone.

The resistance and/or susceptibility to slow crack growth can be quantified by determining and comparing the slow crack growth parameter, n, for c-axis sapphire and YAE. For a given system (environment, temperature, and material), there is a unique relationship between the crack velocity, v, and crack tip stress intensity factor, K_I. An empirical equation that has been used by Wiederhorn[12] to describe the slow crack growth of ceramics can be written as: $v = V_0\left(K_I/K_{I_0}\right)^n$, where K_{I_0} is the threshold stress intensity factor below which crack growth is negligible ($V_O<10^{-10}$ m/s), n is an empirical constant, and V_0 is the crack velocity at $K_I = K_{I_0}$. At equivalent failure probabilities;

$\log\sigma_2 = \log\sigma_1 - \frac{1}{(n+1)}\log\left(\frac{\dot{\varepsilon_1}}{\dot{\varepsilon_2}}\right)$, where σ_i is measured at strain rate $\dot{\varepsilon_i}$, i =1 and 2. The slow crack growth parameter, n, was calculated from $\log\sigma_i$ versus $\log\dot{\varepsilon_i}$. The systematic error due to the uncertainty of absolute strain rate measurement does not introduce large errors in the calculation, because the slow crack growth parameter n is being determined from the ratio of at least two different strain rates. The slow crack parameter for YAE eutectic was large ($n \geq 100$) whereas n for c-axis sapphire at the same conditions was only 12. This corroborates the superior resistance of YAE eutectic to slow crack growth at 1100°C when compared to c-axis sapphire. Limited slow crack growth contributes to greater retention of tensile strength at elevated temperatures.

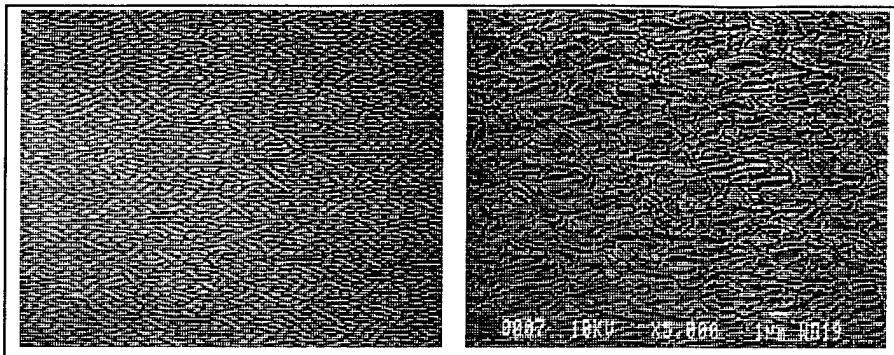

Fig. 2 Surface of YAE. The primary fracture origin in this fiber was at the fiber surface, opposite a well-aligned plate-like "*Chinese Script*" microstructure (left micrograph) which correlated with residual compressive stresses. Away from the thin area a coarser, more random structure was observed (right micrograph).

It is however known that the exponent n is effected by residual stresses[13] and is dependent on whether it is determined from artificial microcracks or from natural cracks.[14] In the absence of any theoretical work related to slow crack growth characteristics of directionally solidified eutectic ceramics, the time to failure of YAE eutectics needed to be determined experimentally. The time to failure under static loading was examined at 1100 °C and results was examined at 1100 °C and results shown in Fig. 4. Directionally solidified YAE eutectic sustained loads of at least 0.89 GPa without failure at 1100 °C in vacuum. Sapphire fails within 100 hours at 0.62 GPa. Furthermore, residual room temperature tensile strengths of stress rupture survivors were similar to strengths of as-received fibers. Hence, YAE eutectic also exhibit superior time to failure under static loading conditions compared to single crystal c-axis sapphire. However, there was an apparent difference in stress levels between dynamic loading (1.35 GPa; Fig. 3) and static loading (0.89 GPa; Fig. 4) conditions. This suggests that, in addition to the slow crack growth parameter, n, the threshold stress intensity factor, K_{Io}, has a profound effect on the life-time determination of the material. The experimental and theoretical data of K_{Io} for ceramic eutectics as a function of temperature as well as the intrinsic crack nucleation probability is not available.

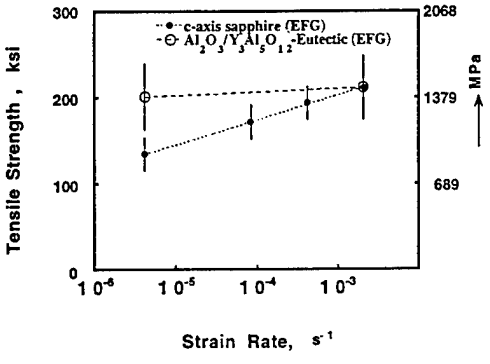

Fig. 3 Time dependency.

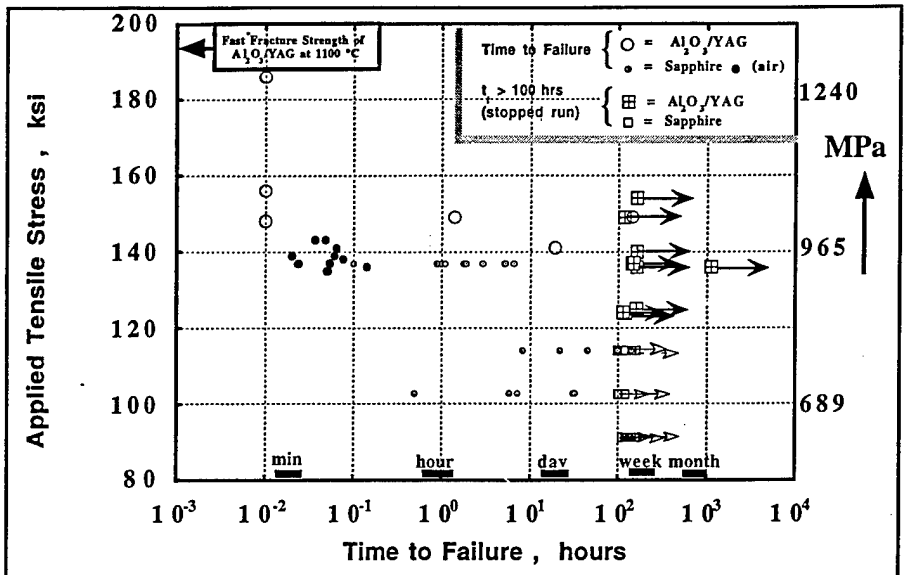

Fig. 4 Time-to-failure of $Al_2O_3/Y_3Al_5O_{12}$ eutectic and c-axis sapphire.

For YAE, typical time dependent creep strain data measured in vacuum are shown in Fig. 5. The creep rate constantly decreases with time, giving the appearance of a primary or transient creep stage up to 0.4 % or more strain. Fiber fracture occurs during this stage at 1100 °C. At 1400 °C, the estimated creep rates are given in Ref. 7. The YAE eutectic has comparable creep resistance to c-axis sapphire, better resistance than a-axis Al_2O_3 but is not as good as single crystal $Y_3Al_5O_{12}$ (YAG).[3] Extensive work in YAE system by Matson et al.[15] determined that the two phase intertwined single crystal morphology would provide higher creep resistance. Matson et al.[16] also investigated coarsening characteristic of this material and found that the inherent homogeneous coarsening was very slow and obeyed the $t^{1/4}$ kinetics.[16] Coarsening of fibrous eutectics has been treated analytically by Ardell[17] and through numerical analysis by Rogers and Desai.[18]

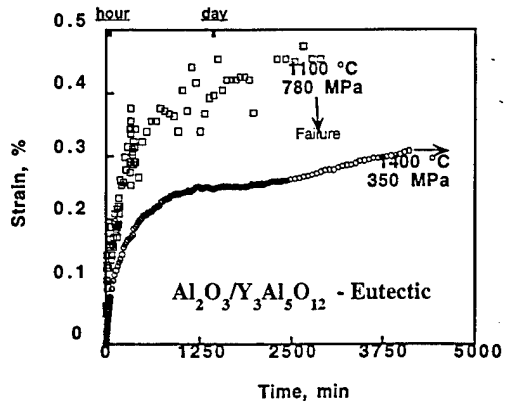

Fig. 5 Creep of $Al_2O_3/Y_3Al_5O_{12}$ at 1400 °C.

The experimental determination of slow crack growth and creep behavior shows unambiguously that the mechanical properties of two phase eutectics can be superior to the properties of either constituent alone due to the strong constraining effects of the interlocking microstructure (Fig. 2). This effect can be unusually high in ceramic eutectics due to the formation of very clean coherent or semicoherent interfaces.[7] However, we currently do not have any clear fundamental theory for directionally solidified eutectic ceramics which will take into account the crack growth characteristic relation to stress intensity factor (K_{max} or ΔK). Thus, prediction of the limits and capabilities of directionally solidified eutectic ceramics is an area that mandates increased attention of theoreticians if these materials are ever to gain acceptance for high temperature structural applications.

2.2. MICROSTRUCTURAL CONTROL OF DIRECTIONALLY SOLIDIFIED CERAMIC EUTECTICS

2.1 Residual Stresses: YAE System

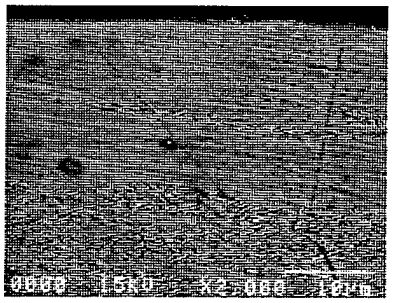

Fig. 6 Cross-section.

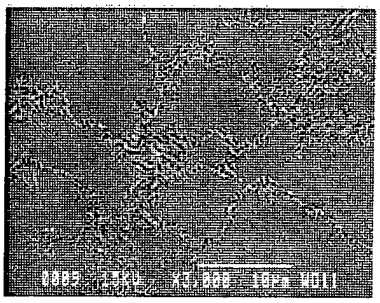

Fig.7 Longitudinal section

In the previous section, the mechanical properties of directionally solidified materials was discussed. The significance of controlled microstructures on mechanical properties should not be underestimated. The microstructures of the YAE was not uniform, made up of multiple of variant regions and regions in which a single variant of the Al_2O_3 phase appeared to dominate, Fig. 6. This morphological substructure is not a result of the cellular structure, because this composition does not develop the cellular pattern even at high rates of growth and low temperature gradients.[7] Figure 7 is a SEM analysis of a TEM thin foil showing that most of the thin area of one of the weaker eutectic contained the "plate-like" structure. However, away from the thin area

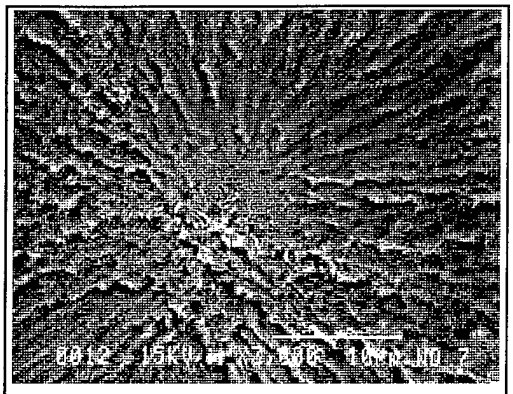

Fig. 8 Fracture origin

a coarser, much less uniform structure was observed. TEM images show the differing structures. There was no large scale faceting of the interfaces in the coarser regions. In the plate-like regions, a sharp interphase boundary is observed.[7] Figure 7 shows the fracture surface morphology of a YAE after stress rupture testing (survived; 0.937 GPa and 1129 hrs). This particular fiber was bent during stress rupture test and after surviving the stress rupture test had a residual room temperature tensile strength of 2 GPa. The primary fracture origin in this fiber was near the fiber surface, opposite a well-aligned plate-like microstructure which apparently was a source of residual compressive stresses (Fig. 8). Based on these observations of microstructure property variations of YAE eutectic, it is concluded that a highly controlled eutectic growth morphology is required to achieve long stress rupture times. The temperature dependencies of thermal expansion coefficients of Al_2O_3 and $Y_3Al_5O_{12}$ are very similar and therefore can not account for the development of the residual stresses. The residual stresses, however, can build up due the modulus mismatches and misfit strains at the interphase boundaries. Three dimensional atomistic models are needed to predict the stress tensors which should take into account the full elastic anisotropy of the phases.[18] Less well understood, but of equal consequence, are intrinsic stress relaxation mechanisms in which the eutectic interacts with an externally applied stress field. In one of our experiments,[21] a remarkable amount of relaxed strain was recovered upon further heat treatment signifying that YAE eutectics can exhibit anelastic behavior. Such recovery of the time dependent strain requires a mechanism which can store elastic stress. A phase-sliding mechanism similar to Zener's grain boundary sliding with accommodation of strain in the lamellae is possible.[22] Variations in the local phase geometry and spatial distribution may also impart highly inhomogeneous local deformation and non-proportional loading.[23] Realistic analyses which take into account the unique phase geometries of ceramic eutectics are needed. The complexities of different microstructures, combined with atomistic models of interphase boundaries to predict the stresses, may require numerical approaches.

3.3 Residual stress measurements on YAE Eutectic (Dr. E. Dickey[23])

In previous sections, the mechanical properties of directionally solidified materials were described. The significance of controlled microstructures for mechanical properties should not be underestimated. In the preliminary studies of mechanical properties, microstructural features which limit strength and/or stress rupture properties have been identified. For example, the microstructures of the YAE used in some stress rupture tests consisted of a mixture of multiple Al_2O_3 variant regions and regions in which a single variant of the Al_2O_3 phase appeared to dominate. This morphological substructure cannot be attributed to cellular growth front structure, because this composition does not develop the cellular pattern even at high rates of growth and low temperature gradients.

Property	YAG	Al_2O_3
Crystal Class	cubic	trigonal
CTE ($x10^{-6}$ / C)	8.9 [23]	a: 9.1 [22] c: 9.9
Elastic Constants : C_{11}	334 GPa[26]	495 GPa [26]
C_{12}	112 GPa	160 GPa
C_{44}	115 GPa	146 GPa C_{33} = 497 GPa C_{13} = 115 GPa C_{14} = -23 GPa
Zener Ratio: $2C_{44}/(C_{11}-C_{12})$	1.04	—

Table.1 Compilation of crystal properties.

SEM analysis of a TEM thin foil showed that most of the thin area of one of the weaker eutectic fibers contained a "plate-like" or tabular structure. However, away from the thin area a coarser, much less uniform structure was observed. There was no large scale faceting of the interfaces in the coarser regions. Thus, the coarser regions with Chinese script microstructure may contain residual stresses which may be responsible for strength reduction. Residual stress measurements were made on YAE DSE with Chinese script microstructures that was grown by laser heated float zone (LHFZ) method. Ultimately these measurements not only give a reasonable estimate of the residual stress but, when compared to theory, give information about the degree of interfacial constraint between the two phases.

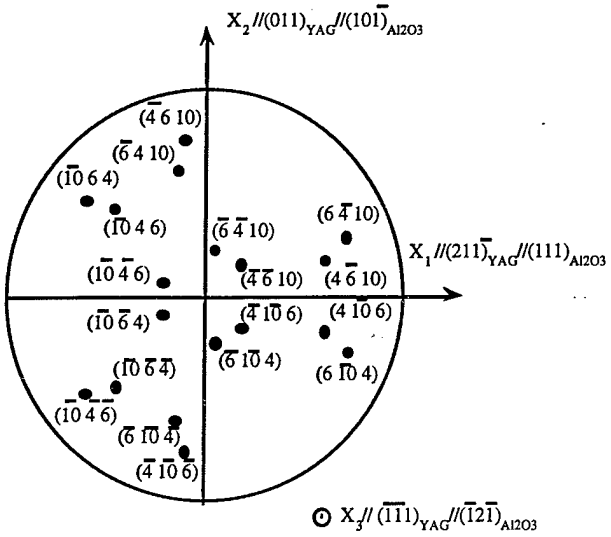

Fig. 9 Streographic projection showing the 18 {10 6 4} reflections used to measure the residual strain tensor of YAG in a $Al_2O_3/Y_3Al_5O_{12}$(YAG) DSE.

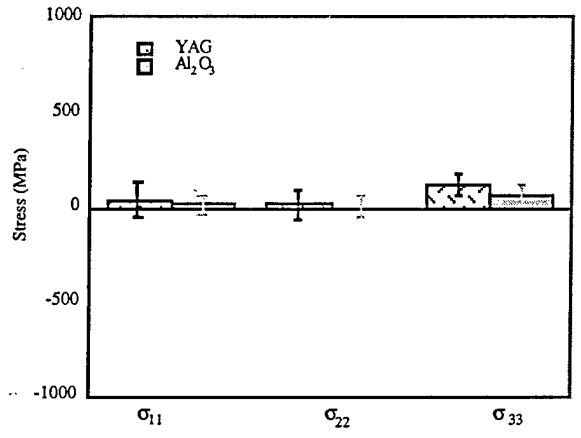

Fig. 10 Cumulative stress results for $Al_2O_3/Y_3Al_5O_{12}$.

One reason that YAE composites are good candidates for high-temperature structural materials is that the thermal expansion properties of the constitutive phases are very similar. One of the microstructure of these composites is typically of the Chinese-script type, so the stress state will necessarily be more complex than that of the ideal lamellar or fibrous microstructures. The other complicating factor is that alumina is not cubic so both its thermal expansion and elastic properties are anisotropic. YAG on the other hand is cubic so its thermal expansion tensor is fully isotropic. As shown in Table I, the Zener ratio of YAG is 1.04, so it is also nearly elastically isotropic as well.

Residual stress measurements were made on a YAE DSE approximately 2 mm in diameter that was grown by the laser-heated floating zone (LHFZ) method. The orientation relationships found in these crystals were consistent with those previously published in the literature, although the growth direction was different. Although only one orientation of YAG was found in the sample, two twin-related variants of Al_2O_3 were found. The variants were:

$[\bar{1}\,\bar{1}\,1]_{YAG}$ // $[\bar{1}2\bar{1}]_{Al_2O_3}$ // growth direction

and

$(2\bar{1}\,1)_{YAG}$ // $(111)_{Al_2O_3}$

or

$(2\bar{1}\,1)_{YAG}$ // $(\bar{1}\,\bar{1}\,\bar{1})_{Al_2O_3}$

The resulting stress tensors for the two phases are presented below with the reference frame outlined in Fig.9 above[23]:

YAG:

$$\begin{bmatrix} 43 & -26 & -71 \\ -26 & 18 & -111 \\ -71 & -111 & 119 \end{bmatrix} \pm \begin{bmatrix} 89 & 36 & 32 \\ 36 & 78 & 40 \\ 36 & 40 & 58 \end{bmatrix} \text{MPa}$$

Al_2O_3:

$$\begin{bmatrix} 16 & -72 & 21 \\ -72 & 3 & -18 \\ 21 & -18 & 67 \end{bmatrix} \pm \begin{bmatrix} 137 & 34 & 54 \\ 34 & 136 & 33 \\ 54 & 33 & 118 \end{bmatrix} \text{MPa}$$

Here x_3 is normal to the sample (parallel to the growth axis; Fig.9. The measured residual stresses in YAE are two orders of magnitude less than those observed in $NiO\text{-}ZrO_2$,[23] and most are approaching the magnitude of the experimental error and are therefore not statistically significant; Fig. 10.

Residual stresses in directionally solidified ceramic eutectics arise from the thermal expansion mismatches between the two constituents. For a given DSE system, it is difficult to control the residual stress state, since neither the volume fraction of both phases nor their crystallographic orientation relationships can be controlled. Because there are few degrees of freedom, if low residual stresses are important, it is necessary to choose eutectics in which the two phases have similar thermal expansion behaviors. Such is the case for YAE in which the thermal expansion properties are within approximately 5% of each other. Residual stress measurements by x-ray diffraction, presented above, indicate that no significant stresses are present at room temperature.

In conclusion, YAE is an example of a eutectic composite in which the two phases have very similar thermal expansion behaviors. X-ray diffraction measurements indicate that there are no appreciable residual stresses in these composites at room temperature. This is because the thermal expansion mismatch of the two eutectic phases is very small. It should be pointed out that the x-ray results reveal the average stress state of the material. The stress state at less uniform areas (Fig. 7) would be different. Furthermore, the residual stresses can build up due the modulus mismatches and misfit

strains at the interphase boundaries. Our efforts focused on a conceptual approach of examining two phase material systems across a broad compositional and therefore microstructural range which includes but is not limited to eutectic growth (i.e. off-eutectic and eutectic materials).

3.4 Off-Eutectic Compositional Studies:

Laser heated float zone (LHFZ) is being used as a means to efficiently produce and record the underlying growth phenomena associated with two phase structures. Our studies focused on the off-eutectic alumina-YAG system over the range of compositions shown in Table 2. Processing parameters were systematically varied in order to explore the limits of microstructural control and the variety of structures which can be achieved. Figures 11-13 represent recent results on microstructural control and the variety of structures which can be consistently achieved. The effects of superheat and axial temperature gradients, had to be defined and controlled experimentally to achieve reproducible results. Thus, a single eutectic growth morphology can be achieved. This is extremely encouraging and it is expected that this will translate better high temperature structural performance and better stress rupture times than shown in Fig.2. Our efforts are also focused on the characterization of the mechanical properties of this class of materials.

In eutectics grown in non-equilibrium conditions, facet geometries may depend on the anisotropy of interfacial free energy and on the anisotropy of crystal growth kinetics. Data on the faceting behavior of the Y_2O_3-Al_2O_3 candidate materials range from scarce to nonexistent. Faceting in certain materials may be strongly dependent on atmosphere and/or impurity content, and it is an objective of this work to determine how to make use of this to eliminate problems stemming from faceting of the

Weight Fraction Y_2O_3	Molar Fraction YAG	Volume Fraction YAG
0.196	0.082	0.31
0.296	0.156	0.48
0.356	0.226	0.59
0.463	0.426	0.79

Table. 2 Studied off-eutectic compositions.

materials. Striking changes in microstructure can be obtained by altering surface interfacial energies through the addition of dopants. Our recent work with the selective use of dopants has demonstrated the possibility of significantly enhancing fracture behavior and resulted in unique fracture surfaces resembling composites.

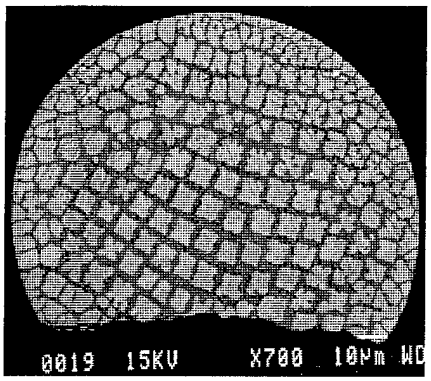

Fig. 11 SEM: rod structures, white phase is YAG.

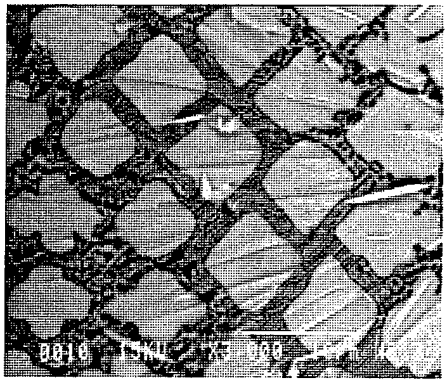

Fig. 12 Between the YAG is two phase eutectic.

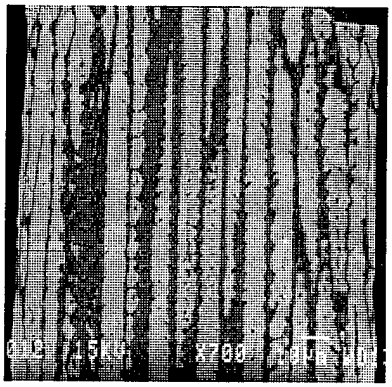

Fig. 13 Longitudinal.

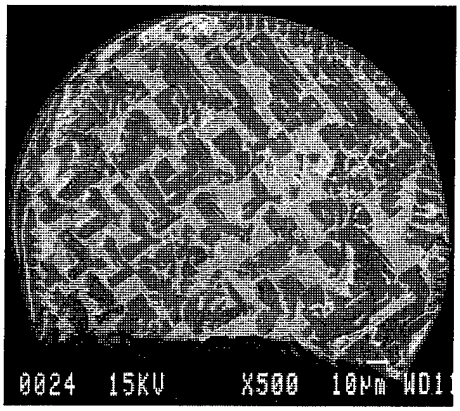

Fig. 14 SEM: plate structures, black phase is Al_2O_3.

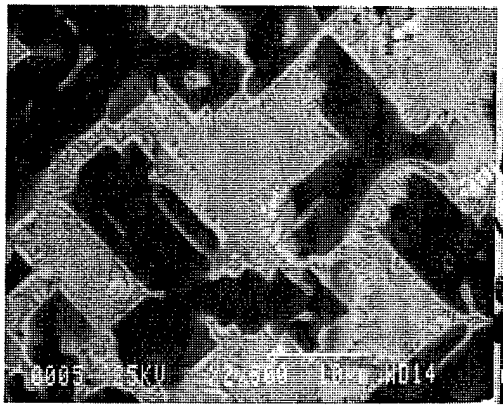

Fig. 15 Between the Al_2O_3 is two phase eutectic.

Fig. 16 Combined cross-section longitudinal view.

The degree of anisotropy, although a necessary condition in promoting improvements in high temperature mechanical properties, is insufficient to achieve higher toughness materials because the bonding between the phases of ceramics is strong. Furthermore, the fine eutectic lamellae will have little effect in diverting the path of the fracture crack. It is however conceivable that through incorporation of controlled amounts of primary phase, for example, the fracture energy of a brittle matrix could be increased. The protruding plates or rods may promote crack deflection at the interfaces between eutectic and primary phase.

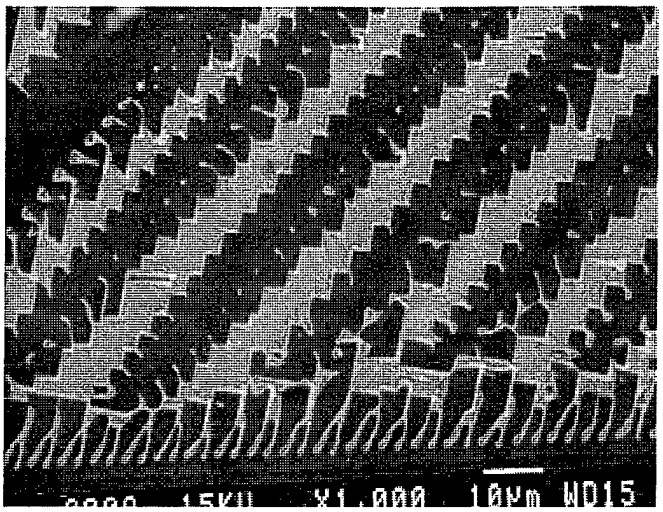

Fig. 17 Faceted view in longitudinal section.

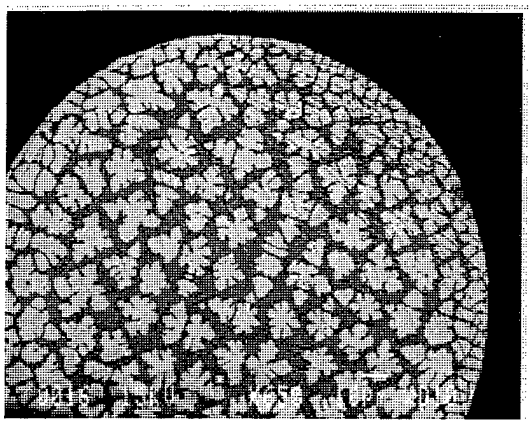

Fig. 18 Dendrites; $Al_2O_3/Y_3Al_5O_{12}$ (off-eutectic).

The directionally solidified metal eutectics provide a large number of fracture examples in which rods protrude.[24] In spite of the fact that extensive theoretical and experimental work has been published in the metal literature on the growth rate of dendrites and faceted growth there is still no unifying theory available.

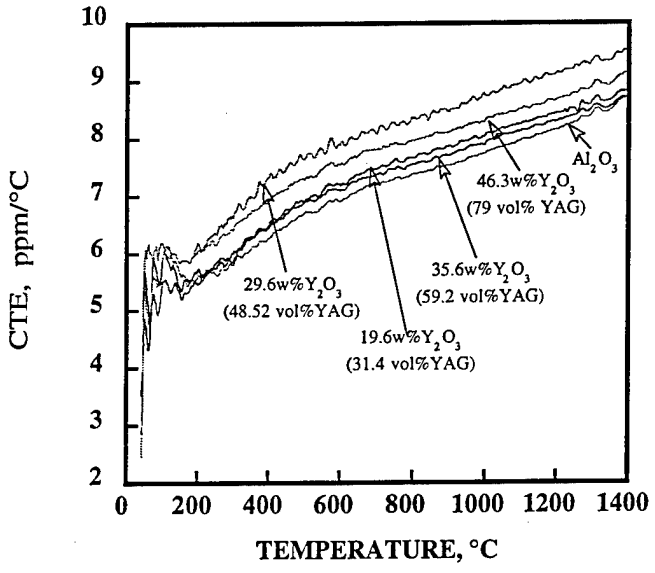

Fig.19 Coeefficient of thermal expansion as a function of second phase (YAG) concentration.

The comprehensive results presented in previous sections unambiguously established the favorable mechanical performance of the eutectic composition. The average tensile strength of Al_2O_3-rich eutectic composition were 2.1 and 1.9 GPa for the 31.4 vol% YAG and 48.8 vol% YAG compositions respectively. The average tensile strength of the YAG rich composition was 1.15 GPa for a 79 vol% YAG

composition. These trials were performed using LHFZ method and resulted in 2 - 3 mm rods with reproducible microstructures similar to shown in Figs. 11 to 18. These rods then have been used to measure the thermal expansion coefficients. The results are shown in Fig. 19 as a function of second phase concentration vol% YAG.

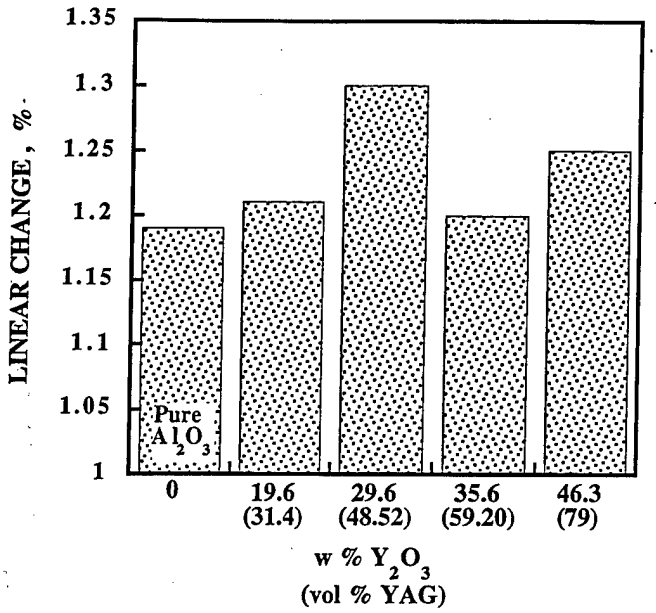

Fig. 20 Linear change (%) of the thermal expansion.

A clear explanation of the strength dependence on the volume fraction of the second phase is currently under study and understanding is not complete. Figure 19 however indicates that at elevated temperatures (T>800 °C) the thermal expansion mismatch increases with increasing temperature. Yet, the mismatch is low, even at elevated temperatures, and therefore can not account for the lower strength values of the YAG-rich compositions. Thus, the modulus mismatch and therefore strains at the interface boundaries would also play an important role to control room temperature tensile strength. However, in engineering applications performance will be dictated on the relationships between lifetime, stress and temperature. Thus, one can conclude that fiber with low volume fraction of YAG-phase would be good for applications which require high temperature strength whereas YAG -rich compositions would perform better where creep requirements are essential. It also should be emphasized that this apparent divergence of the mechanical strength of the fibers also stems from the need to achieve higher toughness in ceramic fibers to withstand the mechanical damage. In short, large aspect ratios and interphase bond integrity characteristics of *in-situ* composites limit the contributions from delamination and emphasize the importance of the matrix contribution to the strength and toughness.

REFERENCES

1. A. Sayir and L. E. Matson, in "HITEMP Review. Advanced High Temperature Engine Materials Technology Program," Proc. of the 2nd Ann. HITEMP Review, October 29- 30, 83 (1991) pp.1-14.

2. A. Sayir, R. M. Dickerson, H. M. Yun, S. Heidger and L. E. Matson, in HITEMP Review Vol. 1 (1994) NASA CP-10146, pp 74.1-74.12.

3. E. Bullock, M. N. McLean, and D. E. Miles, ACTA Metallurgica 25, (1987) 333-344.

4. A. G. Evans Material Science and Engineering 71 (1985) 3-21.

5. V. S. Stubican and R. C. Bradt, Ann. Rev. Mater. Sci., 11 (1981) 267-297.

6. A. Sayir and L. E. Matson, in HITEMP Review Vol. 1 NASA CP-10082, (1992) pp. 83.1 - 83.13.

7. A. Sayir, R. M. Dickerson, H. M. Yun, S. Heidger and L. E. Matson, in HITEMP Review Vol. 1, NASA CP-10146, (1994) pp. 74.1 - 74.12.

8. A. Sayir and S. C. Farmer, in "Ceramic Matrix Composites-Advanced High-Temperature Structural Materials," eds., R. A Lowden, M. K. Ferber, J. R. Hellmann, K. K. Chawla, and S. G. DiPietro, Mat. Res. Soc. Proc., 365 (1995) 11-21.

9. A. Sayir and S. C. Farmer, in "Ceramic Matrix Composites-Advanced High-Temperature Structural Materials," eds., R. A Lowden, M. K. Ferber, J. R. Hellmann, K. K. Chawla, and S. G. DiPietro, Mat. Res. Soc. Proc., 365 (1995) 22-36.

10. S. M. Widerhorn, B. J. Hockey, and D. E. Roberts, Phil. Mag., 28 (1973) 783-795.

11. A. Sayir, in "Advances in Ceramic Matrix Composites," edited by N. Bansal, Am. Ceram. Soc., Westerville, Ohio, (1993) 609-702.

12. S. M. Wiederhorn, Int. J. Frac. Mech., 4 [2] (1968) 171-177.

13. M.V. Swain, J. Mater. Sci., 11 (1976) 2345-2350.

14. X. Hu, Y-W Mai, and B. Cotterell, Phil. Mag., A, 66 [2] (1992) 173-186.

15. L. E. Matson, T. A. Partharsarathy, R. Wheeler IV, unpublished work to be presented at the Ann. Proc. of Ceram. Matrix Comp. and Adv. Ceram. Mater., in Cocoa Beach , Fl., (1998).

16. L. E. Matson, J. M. Yang, F. J. Scheltens, unpublished work to be presented at the Ann. Proc. of Ceram. Matrix Comp. and Adv. Ceram. Mater., in Cocoa Beach, Fl., (1998).

17. A. J. Ardell, Met. Trans., 3 (1973) 1395-1401.

18. T. M. Rogers and R. C. Desai, Phs. Rev., B 39 (1989) 11956-11964.

19. E. C. Dickey and V. P. Dravid, submitted to J. Am. Ceram. Soc., (1997).

20. G. N. Morscher, S. C. Farmer and A. Sayir, Ceram. Eng. Sci. Proc., 16[5] (1995) 959-968.

21. C. Zener, Phys. Rev., 60 (1941) 906-914.

22. Y.-L. Shen, M. Finot, A. Needleman and S. Suresh, Acta. Metall. Mater., 43 [4] (1995) 1701-1722.

23. E. C. Dickey and C. L. Frazer, submitted to J. Eurp. Ceram. Soc.

24. P. Doerner, L. J. Gauckler, H. Krieg, H. L. Lukas, G. Petzow, and J. Weiss, Thermochem., 3 [4] (1979) 241-257.

Appendix III

Final report to Saphikon Inc.

Coarsening of Eutectic Microstructures in a Directionally Solidified $Y_3Al_5O_{12}/Al_2O_3$ Eutectic Fiber

Deok-Yong Park and Jenn-Ming Yang

Department of Materials Science and Engineering
University of California
Los Angeles, CA 90095-1595

Abstract

Coarsening at the surface of directionally solidified $Y_3Al_5O_{12}/Al_2O_3$ (YAE) eutectic fibers has been investigated. The fibers were grown continuously by the edge-defined film-fed growth (EFG) technique. Scanning electron microscopy (SEM) and energy dispersive spectroscopy (EDS) were used to characterize the eutectic lamellar microstructures. Also, electron-probe microanalyzer (EPMA) was used to identify which elements are present in $Y_3Al_5O_{12}$ (YAG) and Al_2O_3 phases. Image analyzer was used to measure the length of the interface between the YAG and Al_2O_3 phases. The difference in the coarsening rate between the surface and the interior region of the $Y_3Al_5O_{12}/Al_2O_3$ eutectic fiber was studied. The coarsening mechanism at the surface YAE fiber was suggested to be by thermal grooving and mass transport along the surface of the fiber (surface diffusion).

1. Introduction

Oxide-based fibers are the most promising materials as the reinforcments for high temperature structural applications in oxidizing environments because of their inherent thermal stability. The single-crystal oxide fibers (such as Al_2O_3, $MgAl_2O_4$, $Y_3Al_5O_{12}$, and Y_2O_3-stabilized ZrO_2)[1-4] and oxide-oxide eutectic fibers (such as $Y_3Al_5O_{12}/Al_2O_3$ and $Al_2O_3/ZrO_2(Y_2O_3)$ have recently gained significant interest.[5-8]

Among the single-crystal oxides and oxide-oxide eutectics, the directionally solidified YAG-Al_2O_3 eutectic (YAE) system has been demonstrated as one of the most promising due to its chemical, microstructural, mechanical, and thermal stability. The long term thermo-mechanical stability of these fibers is critical to their use in advanced high temperature composites. There have been a number of studies of YAE fibers which have been published. There are few studies in which the coarsening of the eutectic structure has been included in the study and there have been no papers in which the coarsening at both the surface and in the interior of the YAE fibers have both been investigated. The purpose of the present study is to investigate the coarsening behavior and mechanism of the YAE fibers

Grain coarsening is an issue in the eutectic system and the relative behaviors of the surface relative to the volume could be significant especially as the fiber diameter is reduced and the surface area to volume ratio increases. Reduction of the fiber strength in the eutectic system due to heat treatments at high temperatures has been reported in a number of papers.[9,10] Localized exaggerated coarsening at the surface of the fiber was reported in the EFG $Al_2O_3/ZrO_2(Y_2O_3)$ and YAE fibers after heat treatment at 1400°C in flowing argon. The exact mechanisms leading to the localized abnormal growth on the surface of both types of eutectic fibers have not yet been identified.

2. Experimental procedure

The YAE fibers produced by Saphikon Inc. with a nominal diameter of 75μm were used in this study. The fibers were grown continuously using the EFG technique at a growth rate of 2.03 cm/min. X-ray diffraction (Model 42202, Norelco, North American Philips Company Inc.) was used for the identification of the phases in the fiber. Both the surface and the interior region of the eutectic fibers were examined using scanning electron microscopy (Stereoscan 250, Cambridge, Scientific Instruments Ltd., Cambridge, England) and energy-dispersive X-ray spectrometry (Kevex SIGMA, Kevex Inc. Valencia, CA). Also, Image-Pro Plus (Ver 3.0) was used for measuring the length of the interface between YAG and Al_2O_3 phases. In order to study the thermal stability of the eutectic lamellar microstructures in the fiber and its effect on tensile strength, some of as-fabricated fibers were heat treated at 1460°C ($0.8T_m$) in air for 50, 100, and 200 h, respectively. All the fibers used in this study were unsized. Prior to heat treatment, the fibers were ultrasonically cleaned.

3. Results and discussion

X-ray diffraction analysis indicated that the fiber contained both YAG and Al_2O_3 phases in both as-fabricated and post-heat-treated states. Secondary electron and backscattered electron images of the surface of the as-fabricated fiber are shown in Fig. 1(a) and (b). Also, the backscattered electron images of the longitudinal and transverse sections of the fiber in the as-fabricated state are shown in Fig, 1(c) and (d). The secondary electrons are not sensitive to the atomic number difference between YAG and Al_2O_3 phases, but sensitive to the topography of the surface in the YAG/ Al_2O_3 fiber. Therefore, the eutectic microstructures at the surface of the as-fabricated fiber could not be observed using the secondary electron image. However, the backscattered electrons are sensitive to the atomic number difference between YAG and Al_2O_3 phases. The lamellar eutectic microstructures of the as-fabricated fiber were clearly observed using the backscattered electrons due to the effect of the atomic number contrast between YAG and Al_2O_3

phases. It is obvious that the microstructures of the as-fabricated fiber consisted of a fine eutectic lamellar microstructure with YAG phase (bright) distributed uniformly in the Al_2O_3 phase (dark). The lamellar spacing of YAG/Al_2O_3 eutectic microstructures was measured to be 0.23~0.27 μm. Examination along a longitudinal section of the fiber (the growth direction) revealed that the microstructure was well aligned along the fiber axis but not perfectly.

After heat treatment at 1460°C (80% of eutectic temperature) in air, the size of both YAG and Al_2O_3 phases at the surface and the interior of the fiber increased significantly as shown in Figs. 2 and 3. Severe coarsening of the lamellar structures at the surface and the interior region of the fiber was clearly observed. Also, it is clear that the coarsening rate of YAG and Al_2O_3 phases at the surface of the fiber is much faster than at the interior region of the fiber. The surface grooves at the interface region between YAG and Al_2O_3 phases were developed as shown in Fig. 4. The migration of atoms near the interface between YAG and Al_2O_3 phases moved to the convex side of a curved surface and developed the surface groove. All the three diffusion mechanisms (surface diffusion, interface diffusion, and volume diffusion) might have contributed to the development of the thermal grooving at the surface of the fiber. The main driving force for the thermal grooving is the reduction of the interfacial free energy (reductions in the total surface areas between YAG and Al_2O_3 interfaces) in the eutectic microstructures. The development of the thermal grooving at the surface of a hot polycrystal wherever a stationary grain boundary emerges to intersect the surface has also been suggested.[11,12] The development of the surface grooves at the surface of a YAE fiber is obvious evidence that the coarsening at the surface of YAE fiber is governed by the surface diffusion mechanism.

The change of length of the interface between YAG and Al_2O_3 phases as a function of heat-treatment time is shown in Fig. 5. It is well known that the driving force for the coarsening of the eutectic lamellar structures is the reduction of the interfacial free energy.[13] The decrease of the length of interface near the surface of the fibers is much

faster than that at the interior areas of the fibers. Also, the coarsening rate from the center region to the surface region of the fiber increased gradually as shown in Fig. 3 (C). Even though the thickness of both YAG and Al_2O_3 layers was increased significantly after heat treatment at 1460°C for 200 h, the interior region of the fiber still maintained their eutectic lamellar microstructures. However, the surfaces of the fibers did not maintain their eutectic lamellar microstructures. Complete phase separation between YAG and Al_2O_3 phases was observed near the surface region of the fiber. Thick, separated YAG layers were formed along the surface of the fiber. Also, thick Al_2O_3 layers were developed beneath the YAG layers along the surface of the fiber. The coarsening rate from the center region to the surface region of the fiber was increased gradually as shown in Fig. 3 (c). The coarsening at the surface of the fiber can occur through surface, interface, and volume diffusion, while the interior of the fiber is governed by interface and volume diffusion. The most significant difference between surface and volume diffusion is the aspect of vacancy formation. In general, it is found the measured diffusion coefficient can be expressed as

$$D = D_0 \exp(-\Delta H/kT)$$

with the pre-exponential factor,

$$D_0 = f\, n_c\, \lambda^2\, \nu_0 \exp((\Delta S_m + \Delta S_f)/k)$$

and the activation energy

$$\Delta H = \Delta H_m + \Delta H_f$$

where:

f is the correlation factor (i.e. the fraction of jumps which lead to random work)

n_c is a coordination factor (i.e. $n_c = 12$ for a FCC solid, $n_c = 8$ for a BCC solid)

λ is the interatomic distance

ν_0 is the vibrational frequency of the solid or the Debye frequency

ΔS_m is the activation entropy for vacancy migration

ΔS_f is the activation entropy for vacancy formation

k is Boltzmann's constant

In the above equation, the activation enthalpy of vacancy diffusion consists of two components; ΔH_f-the activation enthalpy for vacancy formation and ΔH_m- the activation

enthalpy for vacancy migration. The vacancy formation energy, ΔH_f, is at least comparable to the vacancy migration energy, ΔH_m, for many solids.[14] Surface diffusion does not require the formation of vacancies due to the unlimited supply of vacancies at the free surface. However, volume diffusion requires the formation of a vacancy for the diffusion of an atom because of no vacancy source at the interior of a solid. In order to diffuse an atom at the interior of a solid, a vacancy should exist near the atom and the atom can diffuse by the exchange of its site with a nearby vacancy. Also, it is well known that the rate of surface diffusion is much faster than that of interface and volume diffusion.[14,15] From Fig. 6, it can be seen that a significant amount of diffusion was required to produce the microstructure. This required a large amount of void formation along the interface between the coarsened YAG and Al_2O_3 layers near the fiber surface. Therefore, surface diffusion is the dominant mechanism for the coarsening at the surface of the fiber. The voids will act as the source of a failure in the fiber and cause the decrease of the tensile strength and in fact, the mechanical properties such as the tensile strength and the Weibull modulus for heat treated fiber are reduced.[9,10]

Because coarsening of the eutectic lamellar microstructures at the interior of the fiber occurred through interface and volume diffusion process during heat treatment of the fiber, the coarsening rate of YAG and Al_2O_3 phases at the interior region of the fibers is much slower than that at the surface region of the fiber. Also, the well-aligned eutectic microstructures along the fiber axis can be retained after heat treatment at 1460°C for 200hrs. This suggests that only the thickness of each layer at the interior of the fiber would be increased after heat treatment at relatively high temperature. The thickening of YAG and Al_2O_3 layers at the interior of the fiber due to interface and volume diffusion had been reported.[9] However, since surface diffusion is the dominant process and much faster than interface and volume diffusion at the surface of the fiber, the morphology of well-aligned eutectic microstructures before heat treatment would start to change as a function of heat treatment time and the microstructure could be unstable against perturbations. Then, spheroidization of the eutectic lamellar microstructure should occur. The spheroidization of the eutectic microstructures have been reported in many eutectic

alloys.[8,16] This spheroidization occurs both at the interior and the surface of the fiber. The rate of spheroidization at the surface of the fiber is much faster than that at the interior of the fiber.

The secondary electron images of the fiber surface after being heat-treated at 1460°C for 200 hours are shown in Fig. 7. The step-growth in the various sizes of YAG phases was clearly observed. The step-mediated growth model of a crystal at the high temperature by surface diffusion were suggested.[17] EDS spectrum of the same area in Fig. 2 (c) indicated that the spectrum consisted of both aluminum and yttrium. X-ray dot map (area scan) also were performed in order to distinguish YAG and Al_2O_3 phases. Aluminum Kα map and yttrium Lα map are shown in Fig. 8 (b) and (c), respectively. It is obvious from the results of X-ray dot map that the YAG phases were grown at the surface of the fiber. The larger YAG phases were grown at the expense of the smaller YAG phases.

4. Summary

From the above results, the following coarsening mechanisms at the surface of a directionally solidified YAE fiber are suggested. At the initial stage of heat treatment at relatively high temperatures, the well-aligned YAG phases at the surface of the fiber start to thicken with the adjacent YAG phases by thermal grooving and surface diffusion. The driving force for the thermal grooving and surface diffusion is the reduction of the interfacial free energy between the YAG and Al_2O_3 phases. Since the rate of the surface diffusion is much faster than that of volume diffusion and the interface diffusion, YAG phases on the surface of the fiber can not maintain their original morphology (well-aligned eutectic microstructures along the fiber axis) and, therefore, spheroidization by the coalescence of the YAG phases occur. Then the interconnected YAG phases are separated into the isolated YAG phases and the complete phase separation between YAG and Al_2O_3 phases occur beneath the isolated YAG phases on the surface. The larger YAG phases continue to grow at the expense of the smaller YAG phases. The driving force for ripening after a long heat treatment is the concentration gradient associated with the difference in vapor pressure over the large YAG phases and the small YAG phases. Finally, the smaller YAG phases shrink and the larger YAG phases grow as a function of time.

References:

[1] J. E. Sheehan, J. Sigalovsky, J. S. Haggerty, and J. R. Porter, Ceram. Eng. Sci. Proc., 14 [7-8] 660 (1993)

[2] K. J. McClellan, H. Sayir, A. H. Heuer, A. Sayir, J. Haggerty, and J. Sigalovsky, Ceram. Eng. Sci. Proc., 14 [7-8] 651 (1993)

[3] G. S. Corman, "Strength and Creep of Single Crystal YAG Fibers"; presented at the 94th Annual Meeting of the American Ceramic Society, Minneapolis, MN, April 12-16, 1992

[4] G. S. Corman, Ceram. Eng. Sci. Proc., 12 [9-10] 1745 (1991)

[5] S. C. Farmer, A. Sayir, and P. O. Dickerson, "Mechanical and Microstructural Characterization of Directionally-Solidified Alumina-Zirconia Eutectic Fibers; P. 167 in In-Situ Composites: Science and Technology, The Metallurgical Society, Warrendale, PA, 1993

[6] E. L. Courtright, J. S. Haggerty, and J. Sigalovsky, Ceram. Eng. Sci. Proc., 14 [7-8] 671 (1993)

[7] H. E. Bates, Ceram. Eng. Sci. Proc., 13 [7-8] 190 (1992)

[8] T. Mah, T. A. Parthasarathy, and M. D. Petry, Ceram. Eng. Sci. Proc., 14 [7-8] 622 (1993)

[9] J-M. Yang, S. M. Jeng, and S. Chang, J. Am. Ceram. Soc., 79 [5] 1218 (1996)

[10] S. C. Farmer, A. Sayir, P. O. Dickerson, and S. L. Draper, "Microstructural Stability and Strength Retention in Directionally Solidified Al_2O_3-YAG Eutectic Fibers" Ceramic Engineering and Science Proceedings, Sept.-Oct. 1995, the 19th Annual Conference on Composites, Advanced Ceramics, Materials and Structures

[11] W. W. Mullins, J. Appl. Phys., V. 28, 333 (1957)

[12] W. W. Mullins, Trans. AIME, V. 218, 354 (1960)

[13] L. D. Graham and R. W. Kraft, Trans. Met. Soc. AIME, V. 236, 94 (1966)

[14] K. N. Tu, J. W. Mayer, and L. C. Feldmann, "Electronic Thin Film Science for Electrical Engineers and Materials Scientists" (Macmillan Publishing Company, New York, 1970)

[15] J. Askill, "Tracer Diffusion Data for Metals, Alloys, and Simple Oxides" (IFI/Plenum, New York, 1970)

[16] M. Mclean, "Directionally Solidified Materials for High Temperature Services" The Metals Society, London, U.K., 1983

[17] W. K. Burton, N. Cabrera, and F. C. Frank, Philos. Trans. Royal Soc. London, Series A. 299 (1951)

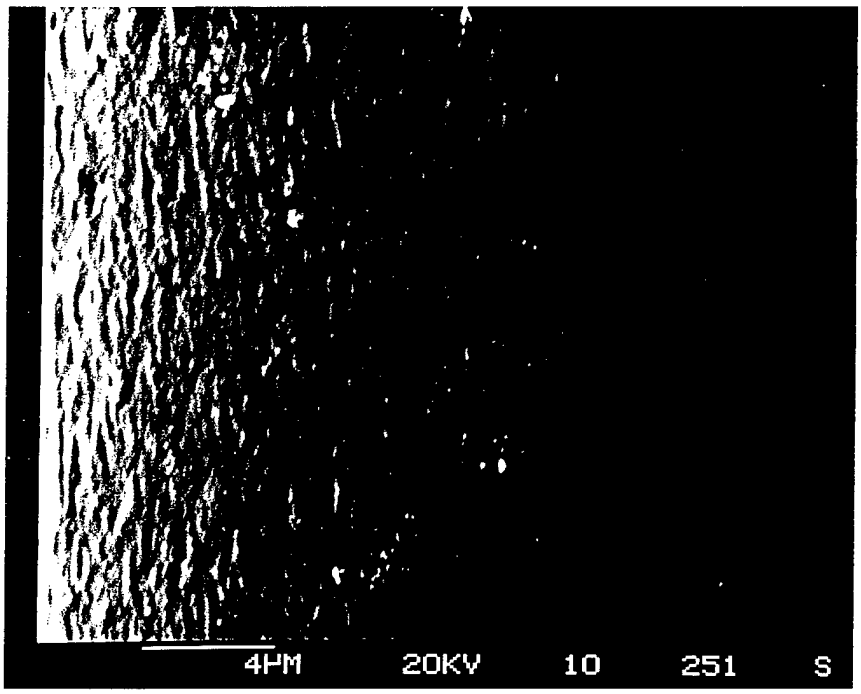

(a)

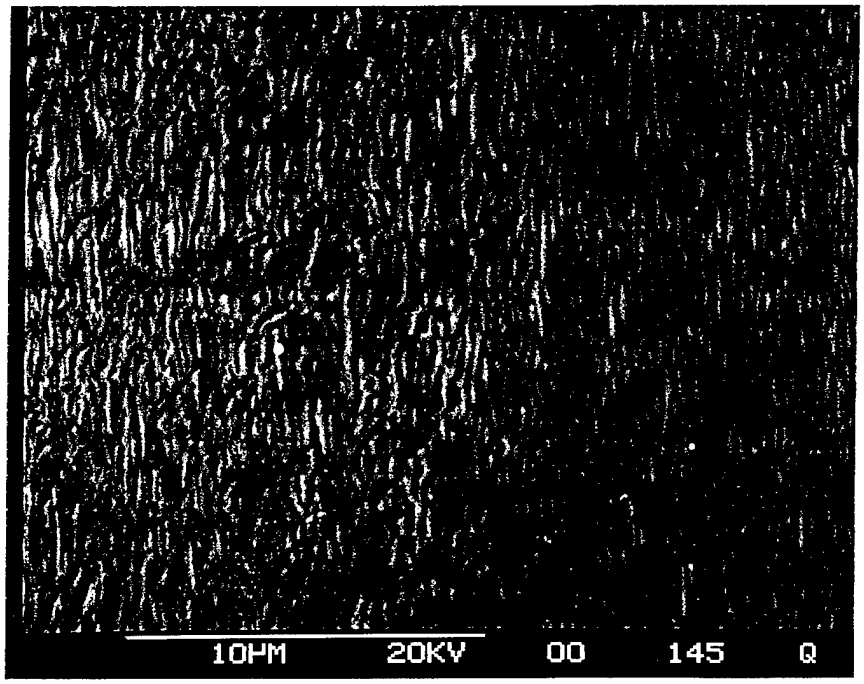

(b)

Fig. 1. The lamellar eutectic microstructures at the surface and interior of the as-fabricated YAG/Al_2O_3 Fiber (Run ID: YAEII- 006-32-7). (a) Secondary electron image at the surface area of the fiber, (b) Backscattered electron image at the surface area of the fiber, (c) Backscattered electron image at the interior area of the fiber (along a longitudinal section), (d) Backscattered electron image at the interior area of the fiber (cross-sectional area).

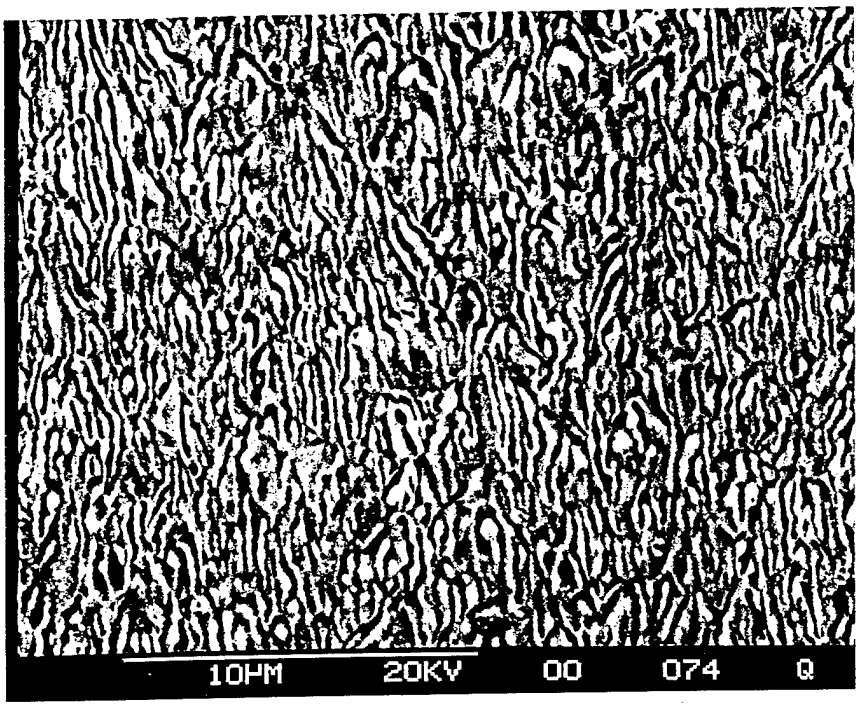

(c)

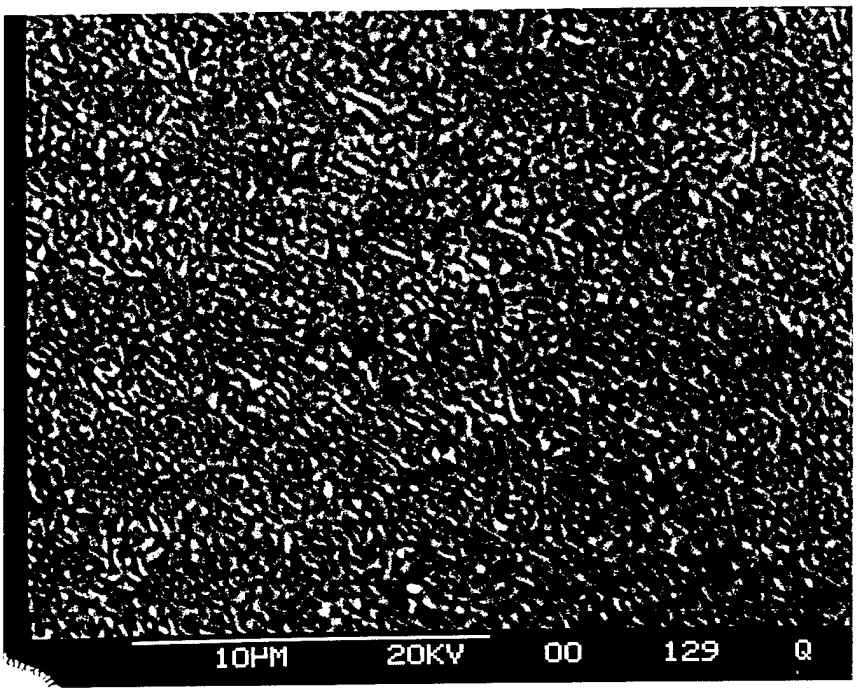

(d)

Fig. 1. Continued

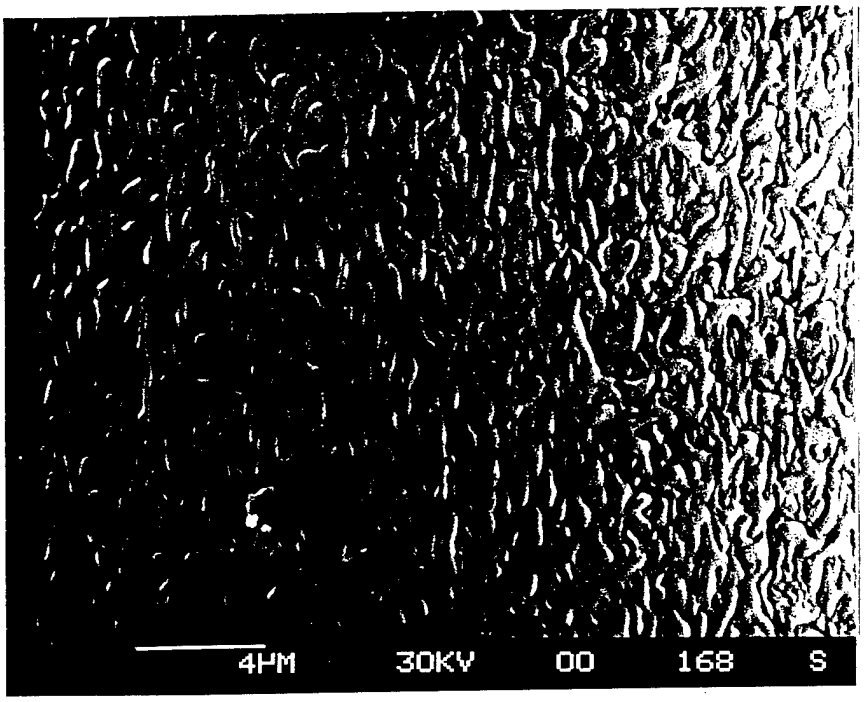

(a)

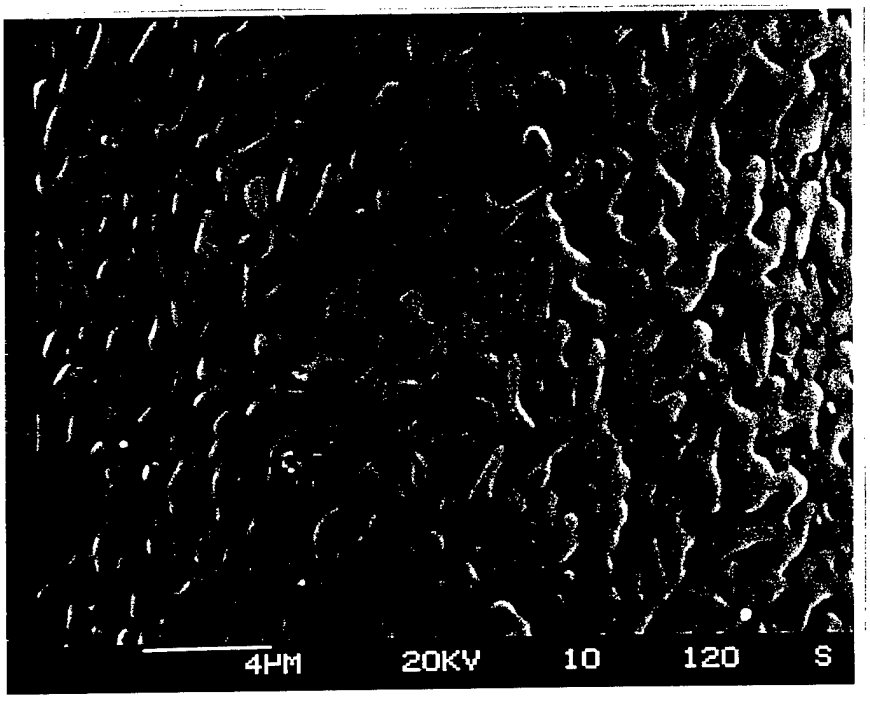

(b)

Fig. 2. The lamellar eutectic microstructures at the surface of the YAG/Al_2O_3 fiber after heat treatment at 1460°C in air (Run ID: YAEII- 006-32-7). (a) for 50hr, (b) for 100hr, (c) for 200hr.

(c)

Fig. 2. Continued

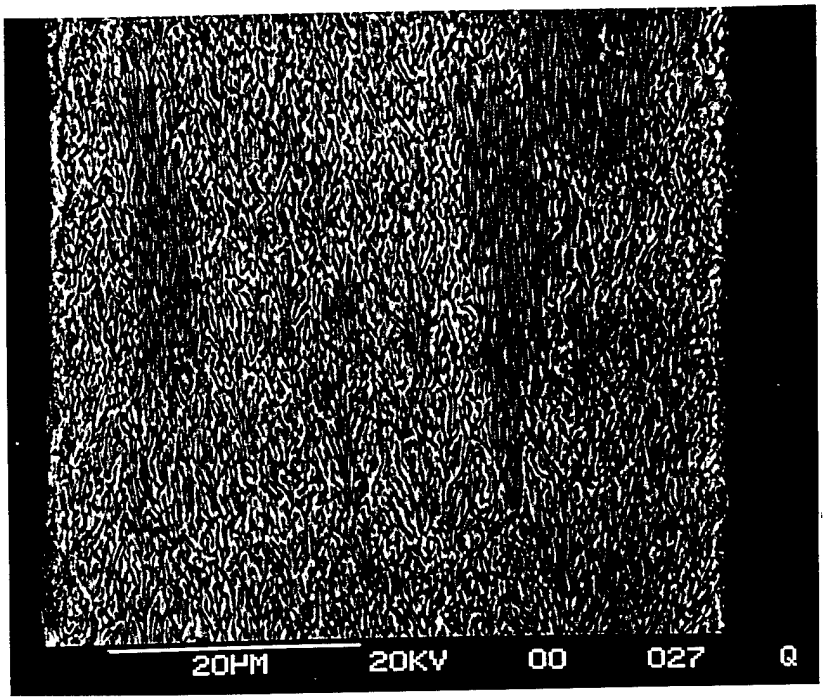

(a)

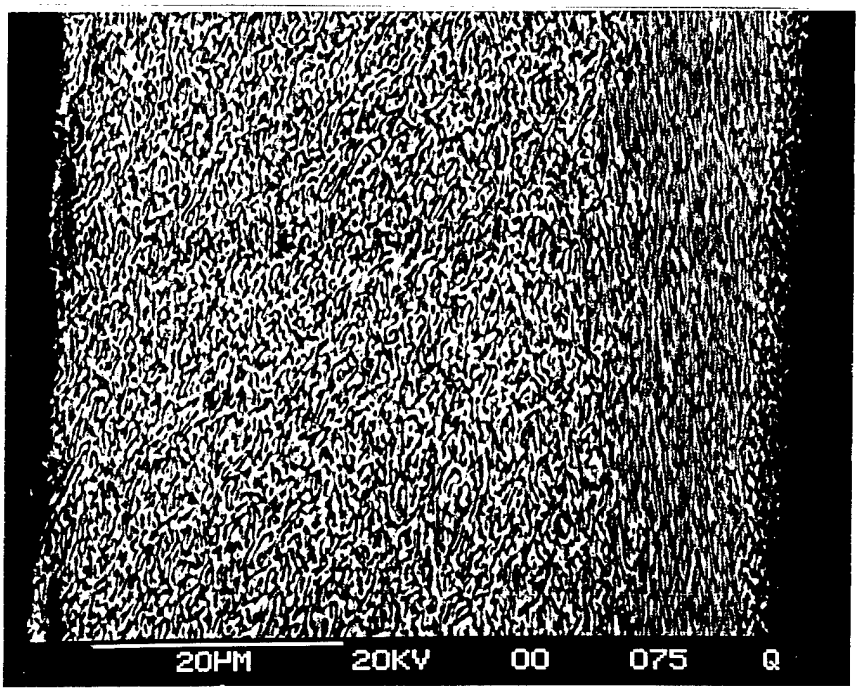

(b)

Fig. 3. The lamellar eutectic microstructures at the interior of the YAG/Al_2O_3 fiber after heat treatment at 1460°C in air (Run ID: YAEII- 006-32-7). (a) for 50hr, (b) for 100hr, (c) for 200hr.

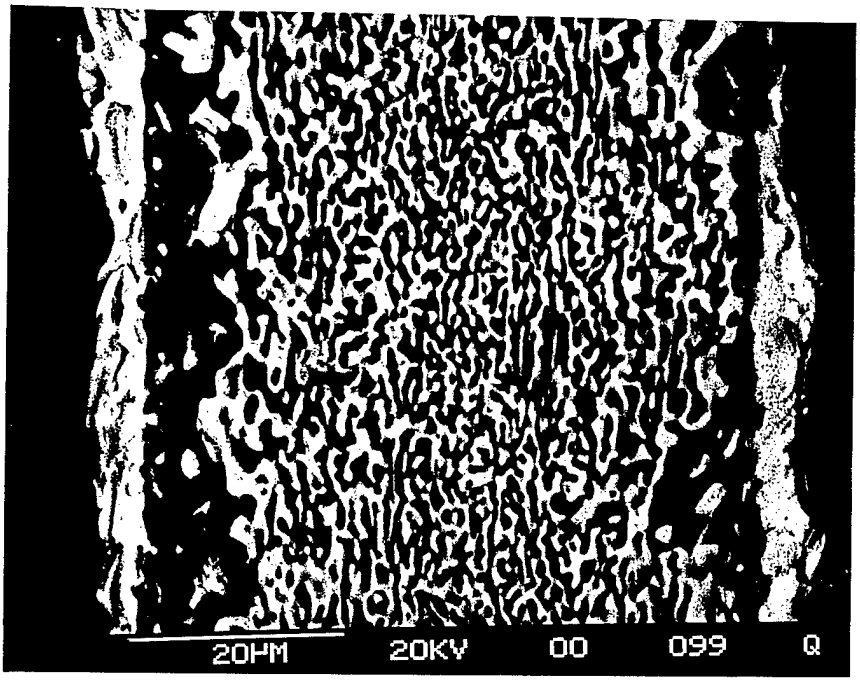

(c)

Fig. 3. Continued

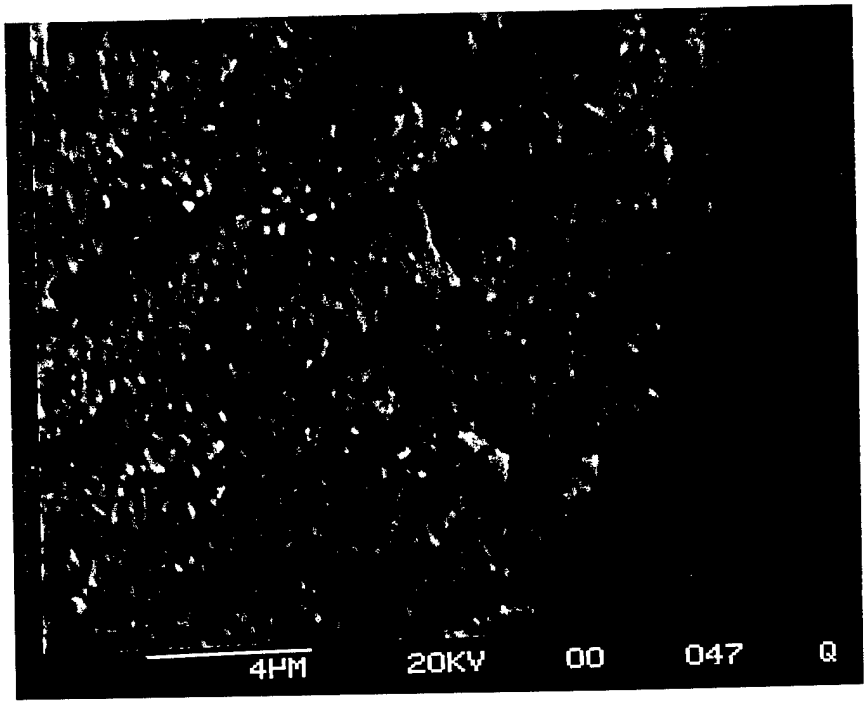

(a)

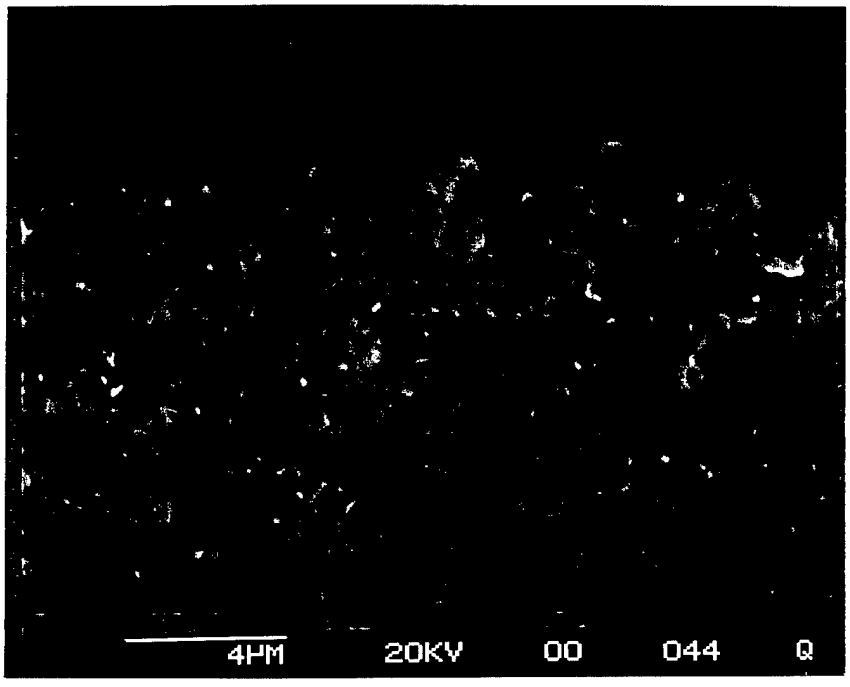

(b)

Fig. 4. Thermal grooves at the surface of the YAG/Al_2O_3 fiber (Run ID: YAEII- 006-32-7). (a) as-fabricated state (b) after heat treatment at 1460°C for 100hr in air.

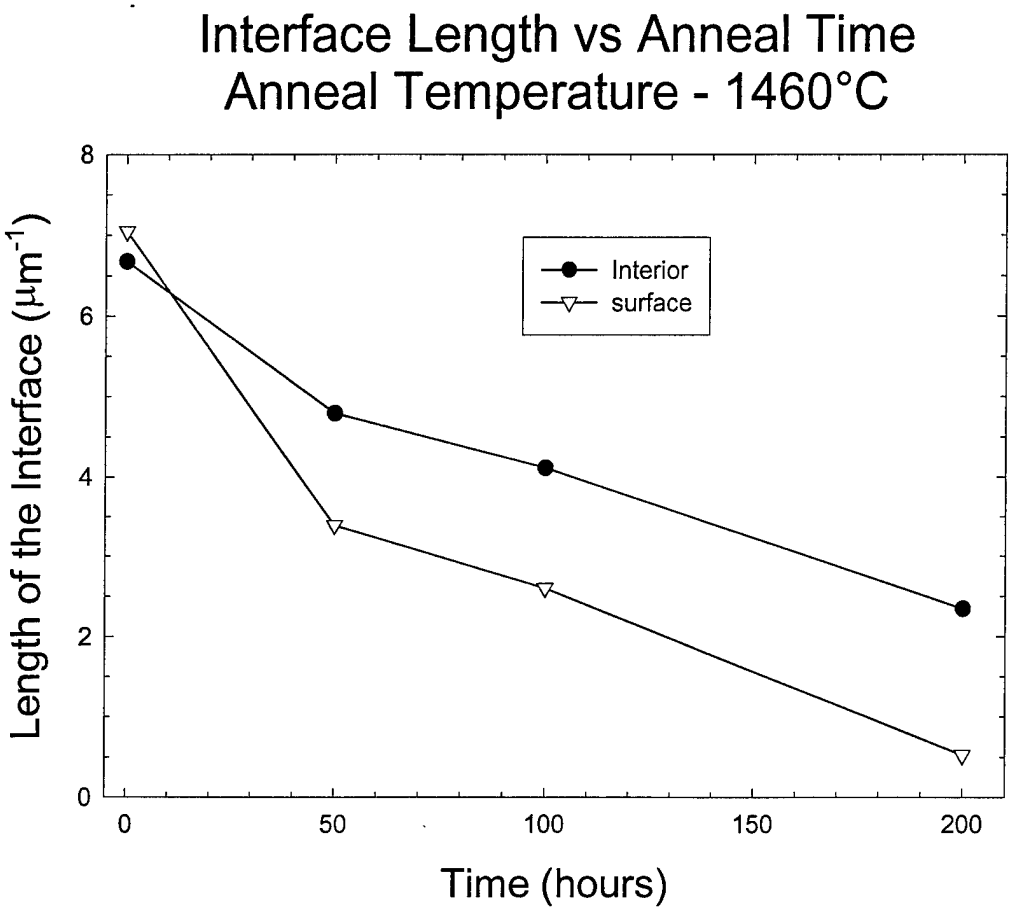

Fig. 5. The change in the length of the interface between YAG and AL_2O_3 fibers as a function of heat treatment time.

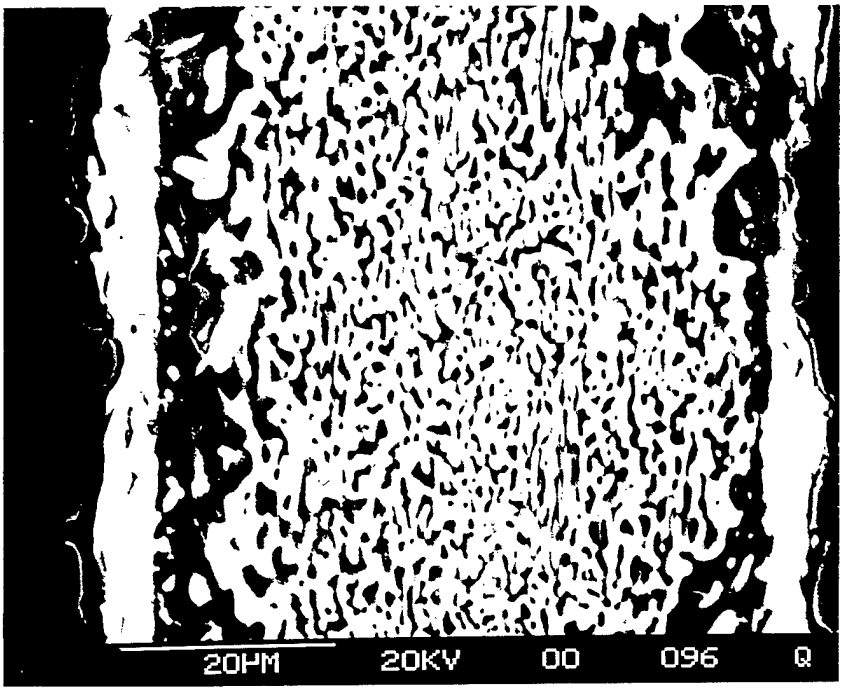

Fig. 6. Voids formation along the thick and separated Al_2O_3 layer beneath the YAG layer at the surface.

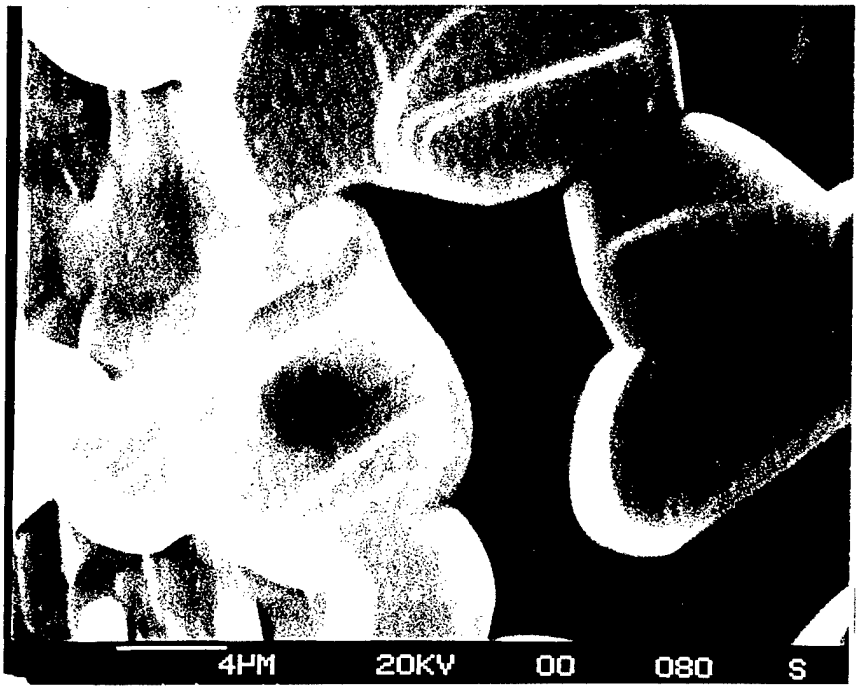

Fig. 7. Step-mediated growth of YAG phase at the surface of the YAG/Al_2O_3 fiber.

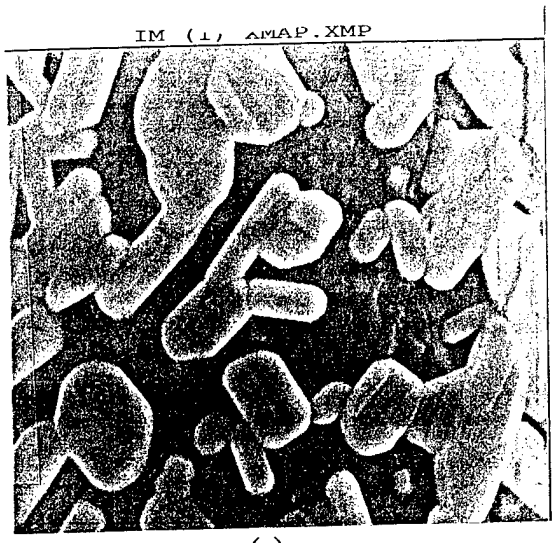

(a)

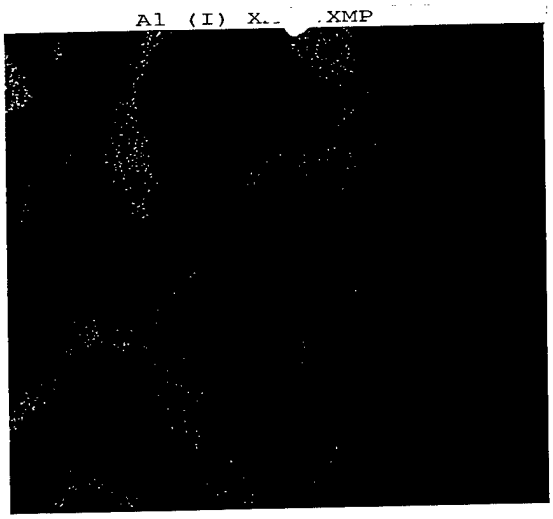

(b)

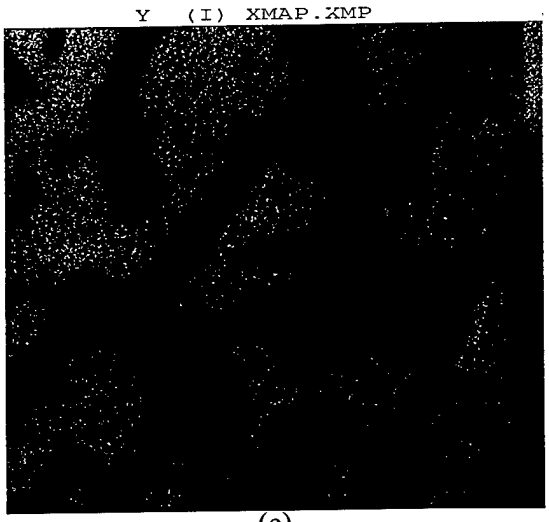

(c)

Fig. 8. X-ray dot map (area scan) of the same area in Fig. 2(c). (a) Secondary electron image of the surface, (b) dot map of aluminum Kα, (c) dot map of yttrium Lα .